UC Irvine
UC Irvine Previously Published Works

Title
Tranexamic Acid-Encapsulating Thermosensitive Liposomes for Site-Specific Pharmaco-Laser Therapy of Port Wine Stains.

Permalink
https://escholarship.org/uc/item/5tk0t7wv

Journal
Journal of biomedical nanotechnology, 12(8)

ISSN
1550-7033

Authors
van Raath, M Ingmar
Weijer, Ruud
Nguyen, Gia Hung
et al.

Publication Date
2016-08-01

DOI
10.1166/jbn.2016.2277

Copyright Information
This work is made available under the terms of a Creative Commons Attribution License, availalbe at https://creativecommons.org/licenses/by/4.0/

Peer reviewed

eScholarship.org Powered by the California Digital Library
University of California

Author Manuscript

Author Manuscript

Author Manuscript

Author Manuscript

HHS Public Access

Author manuscript

J Biomed Nanotechnol. Author manuscript; available in PMC 2017 August 01.

Published in final edited form as:

J Biomed Nanotechnol. 2016 August ; 12(8): 1617–1640. doi:10.1166/jbn.2016.2277.

Tranexamic Acid-Encapsulating Thermosensitive Liposomes for Site-Specific Pharmaco-Laser Therapy of Port Wine Stains

M. Ingmar van Raath[1], **Ruud Weijer**[1], **Gia Hung Nguyen**[1], **Bernard Choi**[2,3,4], **Anton I. de Kroon**[5], and **Michal Heger**[1,5,6,*]

[1]Department of Experimental Surgery, Academic Medical Center, University of Amsterdam, 1105 AZ, Amsterdam, The Netherlands [2]Beckman Laser Institute and Medical Clinic, University of California, Irvine, CA 92617, USA [3]Department of Biomedical Engineering and Surgery, University of California, Irvine, CA 92697, USA [4]Edwards Lifesciences Center for Advanced Cardiovascular Technology, University of California, Irvine, CA 92697, USA [5]Membrane Biochemistry and Biophysics, Institute of Biomembranes, University of Utrecht, 3584 CH, Utrecht, The Netherlands [6]Laser Center, Academic Medical Center, University of Amsterdam, 1105 AZ, Amsterdam, The Netherlands

Abstract

Site-specific pharmaco-laser therapy (SSPLT) is a developmental stage treatment modality designed to non-invasively remove superficial vascular pathologies such as port wine stains (PWS) by combining conventional laser therapy with the prior administration of a prothrombotic and/or antifibrinolytic pharmaceutical-containing drug delivery system. For the antifibrinolytic SSPLT component, six different PEGylated thermosensitive liposomal formulations encapsulating tranexamic acid (TA), a potent antifibrinolytic lysine analogue, were characterized for drug:lipid ratio, encapsulation efficiency, size, endovesicular TA concentration (C_{TA}), phase transition temperature (T_m), and assayed for heat-induced TA release. Assays were developed for the quantification of liposomal TA and heat-induced TA release from two candidate formulations. The outcome parameters were then combined with a 3D histological reconstruction of a port wine stain biopsy to extrapolate *in vivo* posologies for SSPLT. The prime formulation, DPPC:DSPE-PEG2000 (96:4 molar ratio), had a drug:lipid molar ratio of 0.82, an encapsulation efficiency of 1.29%, a diameter of 155 nm, and a C_{TA} of 214 mM. The peak TA release from this formulation (T_m = 42.3 °C) comprised 96% within 2.5 min, whereas this was 94% in 2 min for DPPC:MPPC:DSPE-PEG2000 (86:10:4) liposomes (T_m = 41.5 °C). Computational analysis revealed that <400 DPPC:DSPE-PEG2000 (96:4 molar ratio) liposomes are needed to treat a PWS of 40 cm^2, compared to a three-fold greater quantity of DPPC:MPPC:DSPE-PEG2000 (86:10:4) liposomes, indicating that, in light of the assayed parameters and endovascular laser-tissue interactions, the former formulation is most suitable for antifibrinolytic SSPLT. This was further confirmed with experiments involving *ex vivo* and *in vivo* liposome-platelet and liposome-red

*Author to whom correspondence should be addressed. m.heger@amc.uva.nl.

Disclosure

Michal Heger owns intellectual property rights to SSPLT.

Author Manuscript Author Manuscript Author Manuscript Author Manuscript

blood cell association as well as uptake and toxicity assays with cultured endothelial cells (HUVECs), macrophages (RAW 264.7), and hepatocytes (HepG2).

Keywords

Drug Delivery System; Fibrinolysis; Fluorescamine Derivatization; Heat-Induced Release; Thermosensitive Liposomes

INTRODUCTION

Port wine stains (PWS) are congenital skin lesions characterized by hyperdilated capillaries and post-capillary venules in the dermis. As a result of the microvascular hyperdilation, the affected portion of the skin contains a relatively large blood volume and therefore appears red-to-purple. The lesions, which are located on the face and neck in the majority of patients, generally worsen with age and may be associated with sequelae of psychological and physical nature,[1–4] including glaucoma and seizures.[5–7] The gold standard treatment of PWS is non-invasive laser irradiation, which leads to photocoagulation of the hyperdilated blood vessels.[8] Unfortunately, approximately half of the PWS patients responds suboptimally to laser treatment due to incomplete photocoagulation of the PWS vessels.[9, 10]

Site-specific pharmaco-laser therapy (SSPLT) is a development-stage treatment modality designed to improve the laser treatment of PWS by combining non-invasive laser irradiation with the systemic administration of prothrombotic and/or antifibrinolytic agents encapsulated in a drug carrier.[9–12] The intended clinical effect of SSPLT—the occlusion of incompletely photocoagulated PWS vasculature—emanates from two principal components of endovascular laser-tissue interactions: the photothermal response and the hemodynamic response.[10–12] The photothermal response (Figs. 1(A–C)) entails the conversion of radiant energy to heat by (oxy)hemoglobin and subsequent formation of a thermal coagulum (an amorphous clump of denatured blood) and thermal necrosis of vascular tissue as a result of heat diffusion.[8, 13–15] The hemodynamic response (Figs. 1(D–I)) entails the initiation of primary and secondary hemostasis in consequence to the photothermal response, culminating in the formation of a thrombus.[15] Both responses can lead to prolonged cessation of blood flow in case of complete laser-induced occlusion of the vascular lumen (either by a thermal coagulum, a thrombus, or both), triggering chronic inflammatory processes during which the affected vasculature is removed.[10, 16] Unfortunately, in a large portion of patients the targeted vascular structures are only partially occluded following laser irradiation, which has been correlated to suboptimal clinical outcomes.[17–19] SSPLT was therefore developed,[9–12] to compensate for the incomplete photocoagulation of blood vessels by pharmacologically amplifying the hemodynamic response. The purpose of exacerbating the hemodynamic response is to induce complete occlusion of the PWS vessels through drug-mediated hyperthrombosis and antifibrinolysis (Figs. 1(J–M)), which will ultimately lead to immunological removal of the treated vasculature and hence a good clinical response.

Previously we proposed that tranexamic acid (TA), an antifibrinolytic agent that is widely used in the clinical setting to deter blood loss through its antagonistic effect on

Author Manuscript Author Manuscript Author Manuscript Author Manuscript

plasmin(ogen),[20–24] is a drug candidate for the antifibrinolytic component of SSPLT.[25] The chemical simplicity and small size of TA (MW = 157.2) together with its hydrophilicity and high solubility at physiological pH make this molecule suitable for encapsulation into thermosensitive liposomes. Liposomal formulations that make use of thermosensitivity as a drug release mechanism have been widely studied in relation to oncological applications,[26–28] and constitute a suitable drug delivery system for SSPLT,[10, 29] given the thermal nature of endovascular laser-tissue interactions.[8] In addition to the 'traditional' thermosensitive liposomes composed of diacyl phosphatidylcholines, lysolecithin-containing thermosensitive liposomes have been found to enhance the release kinetics of compounds such as doxorubicin and calcein.[26] Both types of liposomes may therefore be suitable for SSPLT.

Consequently, six TA-encapsulating liposomal formulations with 1,2-dipalmitoyl-*sn*-glycero-3-phosphocholine (DPPC) as the main component phospholipid were evaluated for their potential applicability in SSPLT. First, an analytical method based on primary amine derivatization with fluorescamine was developed to quantify liposomal encapsulation of TA. Next, TA-encapsulating DPPC liposomes with increasing concentrations 1,2-distearoyl-*sn*-glycero-3-phosphoethanolamine-polyethylene glycol (DSPE-PEG) and lysoPC (1-palmitoyl-2-hydroxy-*sn*-glycero-3-phosphocholine, MPPC) were analyzed for drug:lipid ratio, size, encapsulation efficiency, trapped volume, endovesicular TA concentration, and phase transition temperature (T_m). Moreover, an offline drug quantification method was devised to determine the percentage of heat-induced TA release from thermosensitive liposomes, based on which liposomal TA dosages were interpolated for each formulation to the *in vivo* situation. Finally, experiments focused on *ex vivo* and *in vivo* liposome-platelet and LUVET-red blood cell association as well as uptake and toxicity assays with cultured endothelial cells, macrophages, and hepatocytes were conducted with the candidate formulation to shed light on its pharmacokinetics and toxicology.

MATERIALS AND METHODS

All concentrations listed throughout this manuscript refer to final concentrations unless indicated otherwise.

Materials

DPPC, MPPC, 1,2-distearoyl-*sn*-glycero-3-phosphocholine (DSPC), 1-palmitoyl-2-{6-[(7-nitro-2-1,3-benzoxadiazol-4-yl) amino]hexanoyl}-*sn*-glycero-3-phosphocholine (NBD-PC), cholesterol (chol), and 3β-[*N*-(*N*′,*N*′-dimethylaminoethane)-carbamoyl]cholesterol (DC-chol) were obtained from Avanti Polar Lipids (Alabaster, AL). DSPE-PEG (average PEG molecular mass of 2,000 amu), fluorescamine (4-phenylspiro-[furan-2(3*H*),1-phthalan]-3,3′-dione), HEPES (4-(2-hydroxyethyl)-1-piperazineethanesulfonic acid) sodium salt, sodium chloride (NaCl), citrate-phosphate-dextrose solution (CPD), Triton X-100 (TX100), sulforhodamine B sodium salt (SRB, ~75% purity), and trichloroacetic acid (TCA) were acquired from Sigma Aldrich (St. Louis, MO). TA (4-(aminomethyl)cyclohexane-1-carboxylic acid) and 5(6)-carboxyfluorescein (CF) were purchased from Fluka (Buchs, Switzerland). Perchloric acid, ammonium heptamolybdate tetrahydrate, acetic acid, and

Author Manuscript Author Manuscript Author Manuscript Author Manuscript

tris(hydroxymethyl) aminomethane (TRIS) were purchased from Merck KgaA (Darmstadt, Germany). Ascorbic acid was obtained from Acros Organics (Geel, Belgium). TCA was dissolved in MilliQ at a 50% (w/v) concentration and stored at 4 °C. SRB was dissolved in 1% acetic acid at a concentration of 0.4% (w/v). TRIS was dissolved in MilliQ at a 10-mM concentration without further pH adjustments. All chemicals used were analytical grade.

Liposome Preparation and Characterization

Large unilamellar vesicles prepared by extrusion technique (LUVETs) were prepared in the following compositions: DPPC (formulation 1, *F1*), DPPC:DSPE-PEG (98:2, 96:4, and 94:6 molar ratios) (*F2*, *F3*, and *F4*, respectively), DPPC:MPPC (90:10) (*F5*), and DPPC:MPPC:DSPE-PEG2000 (86:10:4) (*F6*). Phospholipids were dissolved in chloroform and mixed at the desired ratios. The solution was desiccated by evaporation under a stream of N_2 gas and exsiccated for at least 20 min in a vacuum exsiccator at room temperature (RT). The resulting lipid film was hydrated with 318 mM TA in 10 mM HEPES buffer (pH = 7.4, 0.302 osmol · kg^{-1} (Osmomat 030 cryoscopic osmometer, Gonotec, Berlin, Germany)) to a lipid concentration of 5 mM and bath sonicated for 10 min. The mixture was subjected to 10 freeze-thaw cycles and extruded 5 times through 0.2-μm Anopore aluminum oxide filters (Anotop, Whatman, Brentford, UK) at 55 °C. The formulations were stored under a nitrogen atmosphere in the dark at 4 °C until further use.

Unencapsulated TA was removed from the LUVET suspensions by size exclusion chromatography during 4-min centrifugation at 100× g and 4 °C in a 2-mL syringe, containing a gel volume of 2.2–2.5 mL (Sephadex G-50 fine, GE Healthcare, Chalfont St. Giles, UK), loaded with 200 μL of the LUVET suspension. Before sample loading, the column was dried by centrifugation at 900× g for 4 min at 4 °C. The column material was hydrated with physiological buffer (PB) (10 mM HEPES, 151 mM NaCl, pH = 7.4, 0.292 osmol · kg^{-1}). The column material was stored at 4 °C and all chromatography and storage steps were performed on ice.

As an internal control for the gelfiltration efficiency, 200 μL of 318 mM TA in 10 mM HEPES buffer (pH = 7.4, 0.302 osmol · kg^{-1}) was loaded onto Sephadex G50 columns (N = 2 per experiment) and the eluent assayed for TA content as described in Section Spectrofluorometric Quantification of Tranexamic Acid. The mean±SD TA concentration in the eluent of control columns was 7.5 ± 0.1% of the loaded liposomal TA concentration (N = 30).

Phospholipid concentrations were determined by the phosphorous assay according to Rouser et al.,[30] and encapsulated TA was quantitated with a spectrofluorometer as described in Section Spectrofluorometric Quantification of Tranexamic Acid. After dilution with PB, LUVET size and polydispersity index (PDI) were measured by photon correlation spectroscopy (PCS) at a 90° angle using monomodal analysis (Zetasizer 3000, Malvern Instruments, Malvern, UK).[31] In some cases, the electrokinetic potential (ζ-potential) was measured (Zetasizer 3000).[31] LUVET phase transition temperatures were determined by differential scanning calorimetry (DSC, MicroCal, Northampton, MA) after dilution of LUVETs with PB to a 3-mM final lipid concentration. PB was used as reference.

Author Manuscript Author Manuscript Author Manuscript Author Manuscript

The *F3* LUVETs for the *ex vivo* LUVET-platelet and LUVET-red blood cell (RBC) association experiments (Sections LUVET Interactions with Platelets and LUVET Interactions with Red Blood Cells) were composed of DPPC:DSPE-PEG2000 (96:4, 5 mM final lipid concentration) and prepared as previously described.[32] Phospholipids were dissolved in chloroform and mixed at the indicated ratio. The solvent was desiccated by evaporation under a stream of nitrogen gas and the lipid film exsiccated for 20 min in a vacuum exsiccator at RT. The lipid film was hydrated with 2 mM CF in 10 mM HEPES buffer, pH = 7.4, to a final lipid concentration of 5 mM and bath sonicated for 10 min. The LUVETs were subjected to 10 freeze-thaw cycles and extruded 7× through 0.1-μm polycarbonate membranes (Avanti mini-extruder, Avanti Polar Lipids) at 80 °C. Directly before incubationwith cells, the extraliposomal CF was removed by size exclusion chromatography (column drying: 900× g for 4min at 4 °C; loading volume: 100 μL; elution: 800× g for7min at 4 °C).

For the LUVETs used in the *in vivo* experiments (DSPC:DPPC:NBD-PC:DSPE-PEG2000, 80:10:5:5, 25 mM final lipid concentration) (Section LUVET Interactions with Red Blood Cells, second test arm), the lipid film was prepared as described in the previous paragraph but hydrated with PBS (10 mM phosphate, 2.7 mM potassium chloride, 137 mM sodium chloride, pH = 7.4, prepared from tablets, Sigma-Aldrich) and bath sonicated for 10 min. The NBD-labeled LUVETs were sequentially extruded through 1.0-, 0.4-, 0.2-, and 0.1-μm polycarbonate membranes (7× per membrane, Avanti mini-extruder, Avanti Polar Lipids) at 80 °C.

For the uptake experiments in cell lines (Section LUVET Uptake by Cultured Cells), *F3* LUVETs were prepared as described above (10 mM final lipid concentration) with the exception that 5 mol% of NBD-PC was incorporated into the LUVETs at the expense of DPPC (DPPC:NBD-PC:DSPE-PEG, 91:5:4) and the lipid film was hydrated with PB that did not contain TA. The LUVETs had a size of 166.0 ± 2.0 nm and a PDI of 0.074±0.027. Moreover, cationic liposomes composed of DPPC:NBD-PC:chol:DC-chol (65:5:5:25, 10 mM final lipid concentration) were prepared as positive control as described by Broekgaarden et al.[31] Lipids were mixed at the desired ratios and the organic solvent was desiccated under N_2 gas at 40 °C. Next, the lipid film was vacuum exsiccated for at least 30 min at room temperature (RT) to remove residual solvent molecules and hydrated with PB. The solution was tip-sonicated until a clear liposome suspension was obtained, after which the liposomes were stored under N_2 gas at 4 °C in the dark. The liposomes were characterized for size and polydispersity as described in Section Liposome Preparation and Characterization and used in experiments within 3 d after preparation.

For the cytotoxicity assays (Section Tranexamic Acid and LUVET Toxicity *In Vitro*), *F3* LUVETs were prepared as described above (DPPC:DSPE-PEG, 96:4, 5 mM final lipid concentration) and hydrated with either PB or 318 mM TA in 10 mM HEPES buffer (pH = 7.4, 0.302 osmol · kg^{-1}). Unencapsulated TA was removed by size exclusion chromatography as described above and lipid content in the eluent was determined by the phosphorous assay as described above.

Author Manuscript Author Manuscript Author Manuscript Author Manuscript

Spectrofluorometric Quantification of Tranexamic Acid

TA was assayed following derivatization with fluorescamine.[33] To demonstrate the conversion of fluorescamine to its fluorophore state in the presence of TA, the absorption (Lambda 18, Perkin Elmer, Wellesley, MA) and fluorescence emission spectra (SPF 500C, American Instrument Company, Silver Springs, MD) were acquired of 7.95 mM TA in 9.96 mM HEPES reacted with 4.5 μM fluorescamine and of 5 μM TA in 5 mM HEPES reacted with 504 μM fluorescamine, respectively. TA and HEPES stock solutions were adjusted to pH = 7.4 prior to mixing with stock aliquots of 1.08 mM fluorescamine in acetone. Reaction mixtures were incubated for 30 min at 37 °C during continuous shaking before spectroscopic analysis. Fluorescence emission spectra were acquired at λ_{ex} = 391±5 nm (the absorption maximum of TA-reacted fluorescamine) and λ_{em} = 483±5 nm.

Regression analysis was performed in order to assess the degree of linearity between TA concentration and fluorescence emission intensity in a predetermined titration range. 500 μL of the TA standard solution (0.0, 1.0, 2.5, 5.0, 7.5, and 10 μM stock concentration in 10 mM HEPES, pH = 7.4) was mixed with 250 μL of 10 mM HEPES, pH = 7.4, and 500 μL of 1.08 mM fluorescamine in acetone (432 μM final concentration). The samples were thermomixed in the dark for 30 min at 37 °C. TA concentration was assayed at λ_{ex} = 391±5 nm and λ_{em} = 483±5 nm.

To rule out any detrimental effects of TX100 on the linear relationship between TA concentration and fluorescence emission and to measure the stability of the fluorophore as a function of time and temperature, TA samples were prepared as above except for the addition of 250 μL of 5% (v/v) TX100 in water (1% final concentration) instead of 250 μL HEPES buffer. Spectrofluorometric measurements were performed immediately following 30-min incubation at 37 °C and after 24-h storage at RT, 4 °C, and −20 °C.

For the spectrofluorometric determination of liposomal TA concentration, the LUVETs were gelfiltered as described in Section Liposome Preparation and Characterization and diluted 500× with PB. 500 μL of the LUVET solution was mixed with 250 μL of 5% TX100 (1% final concentration) and 500 μL of 1.08 mM fluorescamine in acetone (432-μM final concentration). Following 30-min incubation at 37 °C, the samples were assayed at λ_{ex} = 391±5 nm and λ_{em} = 483±5 nm. Reference standards in the 0–4 μM final TA concentration range were included in each separate experiment. Liposomal TA concentrations were derived by solving the regression equation of the reference curve for the respective fluorescence emission intensities. This protocol was used throughout the remainder of the work to determine TA:lipid ratios and to quantify heat-induced TA release.

Calculation Drug:Lipid Ratio, Encapsulation Efficiency, Trapped Volume, and Endovesicular Tranexamic Acid Concentration

Drug:lipid ratios were calculated by dividing the TA concentration as determined by the fluorescamine assay (Section Spectrofluorometric Quantification of Tranexamic Acid), corrected for the gelfiltration efficiency (Section Liposome Preparation and Characterization), by the phospholipid concentration as determined by the Rouser assay (Section Liposome Preparation and Characterization).

Author Manuscript Author Manuscript Author Manuscript Author Manuscript

The encapsulation efficiency, E_{eff}, was computed by dividing the liposomal TA:lipid molar ratio by the initial TA:lipid molar ratio (318 mM TA per 5 mM phospholipid, i.e., 63.6) and expressed as a percentage.

The trapped volume (V_t, L·mole^{-1} lipid) was calculated with the equation (Eq.) obtained from Zuidam et al.[34]

$$V_t=(500/3)(A)(N)(r_v) \quad (1)$$

where A is the area of the membrane occupied by one lipid, N is the Avogadro constant (6.022×10^{23} mol^{-1}), and r_v the mean radius of the vesicle (based on PCS). The areas per phospholipid molecule were obtained from literature: 49.4 Å^2 for DPPC,[35] 50.0 Å^2 for DSPE-PEG,[36] and 48.0 Å^2 for MPPC.[37] For phospholipid mixtures, the areas were weighed averages indexed for the molar ratio of each lipid component:

$$A_{weighed}=[(A_{DPPC})(mol\%_{DPPC})+(A_{DSPE\text{-}PEG})]\times(mol\%_{DSPE\text{-}PEG})+(A_{MPPC})(mol\%_{MPPC})]/100\% \quad (2)$$

The $A_{weighed}$ was 49.4 Å^2 for all MPPC-lacking formulations and 49.3 Å^2 for the MPPC-containing formulations.

The V_t per vesicle (eV$_t$, expressed in L/vesicle) was derived by extrapolating the quantity of phospholipid molecules per vesicle. The quantity of phospholipid molecules per vesicle was defined as the cumulative number of lipids in the outer (l_{om}) and inner membrane leaflet (l_{im}), based on the $A_{weighed}$, the measured mean vesicle size with radius r_v, a bilayer thickness of 3.93 nm,[38] and a spherical morphology (where area sphere = $4\pi r^2$):

$$l_{om}=4\pi r_v^2/A_{weighed} \quad (3)$$

$$l_{im}=4\pi(r_v-3.93)^2/A_{weighed} \quad (4)$$

The eV$_t$ was calculated by:

$$eV_t=[(l_{om}+l_{im})V_t]/N \quad (5)$$

The quantity of TA molecules per vesicle (Q_{TA}) was obtained by multiplying (l_{om} +l_{im}) by the TA:lipid ratio. Subsequently, the endovesicular TA concentration (C_{TA}) was computed from the amount of TA molecules per vesicle for a given eV$_t$:

Author Manuscript Author Manuscript Author Manuscript Author Manuscript

$$C_{\mathrm{TA}} = (Q_{\mathrm{TA}}/N)(1/\mathrm{eV_t}) \quad (6)$$

Heat-Induced Tranexamic Acid Release in Buffer

Heat-induced drug release from TA-encapsulating DPPC:DSPE-PEG (96:4) and DPPC:MPPC:DSPE-PEG (86:10:4) LUVETs was quantified following heat exposure near the maximum T_m and 4 °C below the T_m by a method modified from Huertas-Pérez et al.[25]

The eluent from the first chromatography step was subjected to a second size exclusion chromatography step to ensure complete removal of unencapsulated TA. Prior to heat treatment the gelfiltered LUVET suspensions were diluted 10× with PB that had been kept at 4 °C. 20 μL of the gelfiltered LUVET suspension was diluted 50-fold (N = 3 per experiment) and assayed spectrofluorometrically for total vesicular TA concentration (final dilution factor of 1,250) as described in Section Spectrofluorometric Quantification of Tranexamic Acid. The mean total vesicular TA concentration was used to calculate the percentage of released TA molecules.

Following 5-min equilibration at 4 °C, 160 μL of the LUVETs was transferred into 0.2-mL ultra-thin PCR tubes (Thermowell Gold, Corning, New York, NY) and equilibrated at 4 °C for 10 min before thermally-induced drug release, which was carried out in a thermal cycler (Biozym, Oldendorf, Germany). Samples were heated for a predefined period, after which they were immediately submersed in an ice bath. The entire volume was then transferred to 0.5-mL polycarbonate ultracentrifuge tubes and centrifuged (Optima TLX Ultracentrifuge, TLA 120.1 rotor, Beckman Coulter, Fullerton, CA) at 355,000× g for 90 min at 4 °C to pellet the LUVETs. 50 μL of the supernatant was carefully aspirated and the released TA in the supernatant was quantitated spectrofluorometrically following 50-fold dilution with PB (final dilution factor of 1,250). Phospholipid analysis of the supernatant showed that at least 99.9% of the phospholipids was pelleted. Four untreated 160-μL LUVET samples were included in the ultracentrifugation step to serve as negative control. These samples were processed in the same manner as the heat-treated samples to determine ultracentrifugation-induced TA leakage. The entire protocol is schematically depicted in Figure 2.

TA release was calculated by dividing the mean TA concentration in the supernatant of heat-treated samples by the mean total TA concentration in the LUVETs. TA concentrations were corrected for the mean TA content in the supernatant of the ultracentrifugation control samples.

Interpolation of Liposomal Tranexamic Acid Posology for the *In Vivo* Situation

The interpolation of liposomal TA posology for the *in vivo* situation was based on a three-dimensional reconstruction of a PWS biopsy from serial histological sections as previously described.[39] Briefly, a 3-mm punch biopsy was obtained from a subject with a refractory PWS on the forearm. The tissue was embedded in paraffin, after which 6-μm thick sections were cut and stained with hematoxylin and eosin (H&E). The sections were imaged with a 640 × 480 color CCD video camera at a 20× magnification, whereby three overlapping 2D

Author Manuscript Author Manuscript Author Manuscript Author Manuscript

images were acquired and aligned to reconstruct the entire section in one composite image. Seventy consecutive sections were lined up to comprise the 3D image.

Interactive utilities were programmed for AVS image visualization software (Advanced Visual System, Waltham, MA) as previously described.[40] The programmed utilities combined the images, outlined and stored the position of the epidermal region and vessel circumference, and reconstructed the 3D vasculature from the recorded position of the epidermis and vessels. The lines encompassing the epidermis and blood vessels for each composite 2D image were rotated and translated so that the corresponding regions of consecutive sections coincided. The 3D reconstruction was subsequently composed with standard linear algebra techniques.

The blood volume was derived from a 3D matrix of 358 (depth) × 772 (length) × 70 (number of sections) data points, corresponding to tissue dimensions of 0.716 mm × 1.544 mm × 0.420 mm, respectively. The total dermal volume was quantified from the bottom of the epidermal layer (determined for each column) to the bottom of the section. The blood volume was calculated per 2D section by counting the number of pixels required to fill the regions delineated by the entered vessel circumferences. The cumulative number of 'blood pixels' in the 70 sections hence represented the dermal blood volume.

A blood fraction of 3% was computed in the dermal volume, which comprised 79% of the entire skin specimen. The 3% dermal blood volume most likely represented a lower bound for this specific biopsy region inasmuch as a blood fraction of 4% was calculated when only columns 300–500 of the sections were analyzed. This discrepancy resulted from the fact that the histology section did not have well-defined lateral boundaries. Consequently, a 3.5% dermal blood volume was used in further calculations.

In anticipation of *in vivo* proof-of-concept studies with the TA-encapsulating LUVETs, the minimum number of LUVETs and corresponding lipid concentrations that are required for a systemic TA concentration of 1.9 mM were computed for a 500 μm-long vessel segment of PWS-typical diameters (30–200 μm).[41] The following assumptions were incorporated into the model calculations: approximately 7% of an individual's body weight (BW) is attributable to blood; blood has a specific gravity of 1.060 kg · L^{-1} (vs. 1.000 kg · L^{-1} for water); 55% of whole blood volume is plasma volume, of which 92% is water volume; and the target TA concentration ([TA]) is 10 mg·kg^{-1} body weight,[42] corresponding to a final concentration of 1.9 mM. The number of minimally required LUVETs (L_m) for a vessel segment of length l and radius r, a given percentage of TA release (R_{TA}), and the quantity of TA molecules per vesicle (Q_{TA}) can subsequently be derived by the following equation:

$$L_{\mathrm{m}}=(\pi r^2 l)[TA](N)(R_{\mathrm{TA}})/Q_{\mathrm{TA}} \quad (7)$$

where the corresponding lipid concentration (C_{lip}) is calculated on the basis of the number of lipids in the outer and inner membrane (l_{om}+l_{im}) of a vesicle:

Author Manuscript Author Manuscript Author Manuscript Author Manuscript

$$C_{\mathrm{lip}}=(L_{\mathrm{m}}(l_{\mathrm{om}}+l_{\mathrm{im}})/N)/(\pi\, r^2 l) \quad (8)$$

Since L_{m} and C_{lip} can be calculated for a given blood volume ($\pi r^2 l$), the approximations can be extended to actual PWS if the total quantity of blood per dermal volume is known. Based on the computational analysis, a typical PWS with a surface area of 0.65 mm^2 and a skin volume of 0.46 mm^3 has a dermal volume of 0.39 μL (85% of analyzed skin volume) and a corresponding dermal blood volume of 14 nL, which translates into 2.15 μL blood per cm^2 of skin surface. The number of minimally required LUVETs per μL of blood was then calculated by $L_{\mathrm{m}}/(\pi r^2 l)$ after solving for L_{m} with predefined vessel segment dimensions (vessel with radius, r, and length, l) using Eq. (7). The number of minimally required LUVETs per μL blood is presented for each candidate formulation in Table I.

On the basis of this information, the number of minimally required LUVETs for a PWS, L_{PWS}, was subsequently derived as a function of PWS surface area by solving for:

$$L_{\mathrm{PWS}}=(\mathrm{L_m}\cdot\mu\mathrm{L}^{-1})(2.15\,\mu\mathrm{L}\cdot\mathrm{cm}^{-2})(A_{\mathrm{PWS}}) \quad (9)$$

where ($\mathrm{L_m}\cdot\mu\mathrm{L}^{-1}$) was based on the values in Table I.

LUVET Interactions with Platelets

All animal studies were approved by the institutional review board of the Catholic University of Leuven[32] and all animals were treated in accordance with the National Institute of Health Guidelines for the Care and Use of Laboratory Animals. Male Gold Syrian hamsters (Elevage Janvier, Le Genest Saint Isle, France) were anesthetized with diethyl ether, and blood was drawn from the retro-orbital plexus through a glass capillary into a tube containing 0.31% final concentration sodium citrate (1:9 citrate:blood ratio) (N = 3 animals). Human venous blood was drawn from healthy volunteers into 50-mL tubes containing 0.38% final concentration sodium citrate (1:9 volume ratio to blood) employing an open blood collection system (N = 4 samples).[15] The blood samples were immediately centrifuged at 200× g for 10 min at RT to prepare platelet-rich plasma (PRP). Isolated PRP was counted (Cell-Dyn 1300, Abbott Laboratories, Abbott Park, IL) and diluted with PBS to a concentration of 25 × 10^3 platelets per μL.

PRP (40 μL) was incubated with 1 μL of 10 μg/mL convulxin (CVX, Kordia Life Sciences, Leiden, the Netherlands) in water for 10 min at RT (activated platelets) or without CVX (resting platelets). Subsequently, 10 μL of the CF-LUVET suspension was added to the diluted PRP to a final concentration of 0.70 mM lipid (corresponding to a platelet:lipid ratio of 2.9 × 10^{13} platelets/mole LUVET lipids) and incubated for 30 min at RT in the dark.

Platelets were washed by increasing the volume to 0.5 mL with PBS and centrifugation for 5 min at 288 × g at RT. The supernatant was discarded to remove the unbound CF-LUVETs. Subsequently, hamster platelets were incubated with 5 μL mouse anti-human CD42b monoclonal antibodies (mAbs) (200 μg/mL, clone 11A4, prepared as previously

Author Manuscript Author Manuscript Author Manuscript Author Manuscript

described)[43] for 10 min, and secondarily labeled with 5 μL phycoerythrin (PE)-conjugated $F(ab')_2$ fragments of goat anti-mouse IgG polyclonal antibodies (100 μg/mL, Jackson Immunoresearch, West Grove, PA) for 10 min at RT in the dark. Human platelets were labeled with 5 μL of PE-conjugated mouse anti-human CD61 mAbs (CD61-PE, 16.5 μg/mL, clone Y2/51, Miltenyi Biotec, Bergisch Gladbach, Germany) during 10 min at RT in the dark. Goat anti-mouse IgG-PE (Jackson Immunoresearch) and mouse IgG-PE (clone 203, Immunotools, Friesoythe, Germany) were used as controls. Finally, 0.5 mL PBS that had been stored at 4 °C was added before FACS (EPICS XL-MCL, Beckman Coulter, Fullerton, CA). Ten thousand events were collected in the platelet gate.

The fluorescence emission from CF-LUVETs (λ_{ex} = 488 nm, λ_{em} = 519 nm) was assayed separately for each gelfiltered CF-LUVET batch so as to verify FL1 fluorescence before incubation with PRP.

Data analysis (mean CF fluorescence intensity and percentage of cells in the upper right quadrant) was performed with FCS Express software (De Novo Software, Los Angeles, CA).

LUVET Interactions with Red Blood Cells

LUVET interactions with RBCs were determined in 3 test arms. In the first test arm, the uptake of CF-encapsulating LUVETs was assayed in isolated human (N = 2) and hamster RBCs (N = 2) obtained as described in Section LUVET Interactions with Platelets. The blood samples were immediately centrifuged at 200 × g for 10 min at RT. The platelet-rich plasma was discarded and the RBC fraction was counted (Cell-Dyn 1300) and diluted with PBS to an RBC concentration of 1×10^6 cells/40 μL. Subsequently, 10 μL of CF-LUVETs was added to the 40-μL RBC aliquot in an Eppendorf tube (0.7 mM final lipid concentration) and the mixture was incubated for either 0 min (control) or 30 min at RT in the dark. Following incubation, 500 μL of PBS (RT) was added to each sample and the RBCs were washed once by centrifugation at 250× g for 5 min at RT to remove unbound CF-LUVETs. The supernatant was decanted and the RBC pellet was resuspended in 1 mL of PBS (RT) for flow cytometric analysis.

In the second test arm, LUVET-RBC interactions were determined *in vivo*. Male Syrian gold hamsters were anesthetized by inhalation of a mixture of air:O_2 (1:1 v/v, 2 L/min) and 4% isoflurane (Forene, Abott Laboratories, Queensborough, UK) through a nasal cap. Maintenance anesthesia was achieved by sustained ventilation with a mixture of air and O_2 (1:1 v/v, 2 L/min) and 1.5–2.5% isoflurane. DSPC:DPPC:NBD-PC:DSPE-PEG2000 (85:10:5:5) LUVETs were infused via the subclavian vein in accordance with Heger et al.[15] at a lipid concentration of 125 μmoles/kg in a 500-μL injection volume. Blood samples were collected into a syringe containing 0.38% citrate (final concentration) following jugular vein puncture at t = 15 min and t = 45 min (N = 3 per group) following infusion as well as from a control animal (no LUVET injection, N = 1). The samples were immediately centrifuged at 200× g for 10 min to isolate RBCs. RBCs were washed thrice with PBS by centrifugation at 350× g for 5 min at RT to remove the NBD-LUVETs and assayed by flow cytometry.

Author Manuscript Author Manuscript Author Manuscript Author Manuscript

Samples in both test arms were assayed on an EPICS XL-MCL flow cytometer. Ten thousand events (test arm 1) and 20,000 events (test arm 2) were collected in the RBC gate and examined for CF/NBD fluorescence (FL1 channel; λ_{ex} = 488 nm, λ_{em} = 519 nm). The fluorescence emission from LUVETs (first test arm) and data analysis were performed as described in Section LUVET Interactions with Platelets.

In the third test arm, the effect of TA, *F3* LUVETs, and TA-LUVETs on RBC hemolysis was investigated. The hemolysis assay was modified from Durán-Lara et al.[44] Peripheral blood (10 mL) of 3 healthy volunteers (MIvR, RW, GHN) was collected into a 15-mL polystyrene tube containing CPD at a 1:9 ratio to blood using an open collection system.[15] The RBCs were isolated by centrifugation as described above and diluted with PBS (equilibrated at 37 °C) to a final RBC concentration of 1×10^{12} RBCs per L. Next, 50 μL of TA-, LUVET-, or TA-LUVET-containing solution was added to 450 μL of diluted RBC suspension in a 0.5-mL Eppendorf tube and incubated at 37 °C for 1, 2, or 3 h. The final concentrations were: LUVETs (10 mM lipid concentration in PB, diluted with PB); 1,000, 500, 250, 125, and 62.5 μM final lipid concentration, TA-LUVETs (10 mM lipid concentration in PB, diluted with PB); 1,000, 500, 250, 125, and 62.5 μM final lipid concentration, and TA (318 mM stock solution in 10 mM HEPES diluted with PB); 100, 50, 25, 12.5, and 6.25 μM (N = 2/concentration). After incubation, the samples were centrifuged at 12,000× g for 5 min at 4 °C. Finally, 200 μL of the supernatant was transferred to a 96-wells plate and absorption was measured at 577 nm (BioTek Synergy HT, Winooski, VT). RBC hemolysis was expressed as percentage of total hemoglobin, obtained by treatment of the 450-μL RBC aliquot with 50 μL of 10% TX-100 (1% final concentration) as a positive control (diluted 60-fold in PB before spectroscopic measurement, N = 4 per time point). The extent of hemolysis in a negative control sample (addition of 50 μL of PB to 450 μL of the RBC suspension) was subtracted from the values obtained in the experimental groups. The extent of hemolysis was expressed as $(OD_{sample} - \text{mean } OD_{negative\ control})/(\text{mean } OD_{positive\ control} - \text{mean } OD_{negative\ control}) \times 100\%$.

Passive Release of 5(6)-Carboxyfluorescein from *F*3 LUVETs

F3 CF-LUVETs containing 2 mM CF were prepared as described in Section Liposome Preparation and Characterization. Following preparation, the CF-LUVETs were subjected to size exclusion chromatography to remove unencapsulated CF as described in Section Liposome Preparation and Characterization. All steps were performed at 4 °C or on ice, and all eluents were pooled. A 200-μL aliquot (N = 2) was transferred to a TLA-100 polycarbonate ultracentrifuge tube (Beckman Coulter) that had been equilibrated at 4 °C (negative control, no release). Also, a 200-μL aliquot (N = 2) was transferred to an ultracentrifuge tube (N = 4) to which 13 μL of 15% TX-100 was added (positive control, 100% release). Additional 200-μL aliquots were transferred to ultracentrifuge tubes that had been equilibrated at 37 °C and incubated at 37 °C for 15, 30, 45, and 60 min (N = 2 per incubation time). Following incubation, the samples were placed on ice to stop heat-induced release. The samples were centrifuged as described in Section Heat-Induced Tranexamic Acid Release in Buffer. Finally, 100 μL of supernatant was carefully aspirated and transferred to a 1.5-mL Eppendorf tube. Following addition of 900 μL of MilliQ, samples were measured spectrofluorometrically at λ_{ex} = 493±5 nm and λ_{em} = 519±5 nm.[32] The

Author Manuscript Author Manuscript Author Manuscript Author Manuscript

percentage of release was calculated on the basis of the CF peak integrals (480–650 nm) and expressed as (fluorescence intensity of sample − fluorescence intensity of negative control)/(fluorescence intensity of positive control − fluorescence intensity of negative control)× 100%.

Uptake of 5(6)-Carboxyfluorescein by Red Blood Cells

The uptake of unencapsulated CF by human RBCs was quantified by flow cytometry. Blood was drawn from healthy volunteers and processed as specified in Section LUVET Interactions with Platelets. A 40-μL aliquot containing 1×10^6 RBCs was mixed with 10 μL of CF in MilliQ (0–3.4 μM final concentration) or 10 μL of calcein in MilliQ (0–2.5 μM final concentration) and incubated for 30 min at 37 °C. Following incubation, 500 μL of PBS (RT) was added to each sample and the RBCs were washed once by centrifugation at 250× g for 5 min at RT to remove free fluorophore from the suspension. The supernatant was decanted and the RBC pellet was resuspended in 1 mL of PBS (RT) for flow cytometric analysis.

LUVET Uptake by Cultured Cells

Human umbilical vein endothelial cells (HUVECs) were isolated from fresh umbilical cords obtained at the Department of Obstetrics and Gynecology and processed as described previously.[45] The chords were stored in transport buffer (140 mM NaCl, 11 mM glucose, 4 mM KCl, 0.52 mM Na_2HPO_4, 0.15 mM KH_2PO_4) supplemented with 10 U/mL heparin and 10 U/mL penicillin, 10 mg/mL streptomycin, and 2.5 ng/mL amphothericin B (Lonza, Basel, Switzerland). The umbilical vein was flushed with Ca^{2+}-free solution (142 mM NaCl, 6.7 mM KCl, 3.36 mM HEPES) under low pressure. The end of the vein was closed and the umbilical cord was filled with Ca^{2+}-free solution (66 mM NaCl, 6.7 mM KCl, 4.8 mM $CaCl_2$, 67.1 mM HEPES) supplemented with 40 μg/mL liberase (Roche, Basel, Switzerland) and incubated for 15 min at 37 °C. After incubation with liberase, the vein was flushed with William's medium E (Lonza) supplemented with 20% fetal calf serum (Gibco/Life Technologies, Carlsbad, CA). The HUVECs-containing effluent was centrifuged for 10 min at 180× g and 20 °C. Cells were resuspended in EndoGRO medium (Millipore, Carrigtwohil, Ireland) supplemented with 10% FCS and penicillin/streptomycin (Lonza, 100 U/mL and 100 μg/mL, respectively). Cells were transferred to 25 cm^2 Primaria culture flasks (Becton Dickinson, Franklin Lakes, NJ) and grown under standard culture conditions (humidified atmosphere of 5% CO_2 and 95% air, 37 °C) in EndoGRO medium. Medium was refreshed after 24 h to remove residual erythrocytes. Cells were typically subcultured once a week at a 1:4 ratio in 75 cm^2 culture flasks. HUVECs were discarded after passage 4.

Murine RAW 264.7 macrophages were grown at standard culture conditions in DMEM supplemented with 2 mM L-glutamine (Gibco/Life Technologies), 10% (v/v) fetal calf serum (FCS, Gibco/Life Technologies), and penicillin/streptomycin (100 U/mL and 100 μg/mL, respectively, Lonza). The cells received fresh medium once a week and were typically subcultured twice a week at a 1:6 ratio.

Human hepatocellular carcinoma (HepG2) cells were cultured in HepaRG medium containing 10% FCS, hydrocortisone hemisuccinate (50 μM, Sigma-Aldrich), L-glutamine

Author Manuscript Author Manuscript Author Manuscript Author Manuscript

(2 mM), insulin (5 μg/mL, Sigma-Aldrich), and penicillin/streptomycin (100 U/mL and 100 μg/mL). The cells received fresh medium once a week and were typically subcultured once a week at a 1:25 ratio.

For the uptake experiments, cells were transferred to 24-wells plates at a density of 6.7×10^4 cells/well (HUVECs), 1.7×10^5 cells/well (HepG2 cells) and 1.5×10^5 cells/well (RAW 264.7 macrophages). The cells were grown as described above (500 μL medium/well) to 100% confluence to prevent LUVET adhesion to the material, which would otherwise yield false positive uptake results (unpublished data).

After reaching confluence, the medium was replaced by phenol red-lacking but otherwise fully supplemented medium (450 μL/well) and 50 μL of PB or NBD-LUVETs was added per well to achieve final lipid concentrations of 0, 25, 100, 250, 500, and 1,000 μM (N=4/concentration). The cells were incubated with NBD-LUVETs or NBD-labeled cationic liposomes for 1 h at standard culture conditions, after which the cells were washed thrice with 1 mL of sterile PBS (Fresenius Kabi, Bad Homburg, Germany) equilibrated at 37 °C.

Protein content was determined with a SRB total protein assay.[46] The solutions were prepared as described in Section Materials. Cells cultured in 24-wells plates were fixed by the addition of ice-cold TCA (300 μL/well) and incubated for at least 1 h at 4 °C. Next, the cells were washed 5× with MilliQ and stained with SRB (250 μL/well) for at least 15 min and washed 4× with 1% acetic acid to remove the unbound stain. The plates were dried at 60 °C in an incubator, after which unbuffered TRIS was added (1 mL/well) to dissolve the SRB by gentle swirling. The plate was read with a multi-well plate reader (BioTek Synergy HT) at 600 nm.

NBD fluorescence was measured with a multi-well plate reader (BioTek Synergy HT) at λ_{ex} = 460±40 nm and λ_{em} = 520±20 nm. Fluorescence intensities were normalized to protein content per well (absorption value). Finally, the values per well were normalized to the mean of the 0-μM final lipid concentration group.

Tranexamic Acid and LUVET Toxicity *In Vitro*

HUVECs, RAW 264.7, and HepG2 cells were cultured as specified in Section LUVET Uptake by Cultured Cells using 24-wells plates. After reaching ~70% confluence, the medium was replaced with 450 μL of phenol red-lacking but otherwise fully supplemented medium to which 50 μL of solution containing TA, LUVETs, or TA-LUVETs was added per well. The final concentrations were: TA (318 mM stock solution in 10 mM HEPES diluted with PB); 0, 1, 2, 4, 8, and 16 mM, LUVETs (5 mM lipid concentration in PB diluted with PB); 0, 25, 50, 100, 200, and 400 μM final lipid concentration, and TA-LUVETs (5 mM lipid concentration in PB diluted with PB); 0, 25, 50, 100, 200, and 400 μM final lipid concentration (N=4/concentration). The cells were incubated for 24 h under standard culture conditions, after which the LUVET/TA-containing medium was replaced with fresh, fully supplemented medium. The cells were incubated for an additional 24 h under standard culture conditions. Next, mitochondrial redox state was determined with a water-soluble tetrazolium 1 assay (WST-1, Roche Applied Sciences, 1:25 dilution in FCS-lacking medium, 15 min incubation at standard culture conditions, absorbance read at 450 nm in a multi-well

Author Manuscript Author Manuscript Author Manuscript Author Manuscript

plate reader). Following the WST-1 assay, the supernatant was discarded and the cells were washed thrice with 1 mL of PBS (RT). Next, protein was determined with the SRB assay (Section LUVET Uptake by Cultured Cells).

Statistical Analysis

Statistical analysis (means, standard deviations, linear regression analysis, Pearson's correlation analysis, Kruskal-Wallis tests, and independent two-tailed homo-and heteroscedastic Student's *t*-tests) were performed with Statistical Package for Social Sciences (SPSS, Chicago, IL). The type of *t*-test used was predicated on Levene's test of equal variances. For the *in vitro* liposome uptake and TA and LUVET toxicity *in vitro* data, intergroup and intragroup differences were analyzed with a Kruskal-Wallis test and Dunn's post hoc test. A *p*-value of ≤ 0.05, designated by (*), was considered statistically significant. A *p*-value of ≤ 0.01 is designated by (**) and not significant results by 'N.S.'

RESULTS

Spectrofluorometric Quantification of Fluorescamine-Derivatized Tranexamic Acid

An assay based on primary amine derivatization with fluorescamine was developed for the quantification of liposomal TA in detergent-treated buffered solutions. Fluorescamine, which is non-fluorescent in native state, reacts readily and rapidly ($t_{1/2}$ = 0.1–0.5 s) with primary amines in a 1:1 stoichiometric ratio to yield highly fluorescent moieties (Fig. 3(A)) that can be quantified in the picomolar range. Non-reacted fluorescamine is hydrolyzed ($t_{1/2}$ = 5–10 s) to form non-fluorescent reaction products.[33]

The formation of the fluorophore in the presence of TA was determined spectroscopically inasmuch as changes in chromophore structure are associated with alterations in absorption and fluorescence properties. As shown in Figure 3(B), a shift in the absorption maximum (Δ_{Abs}) from 265 nm (non-reacted fluorescamine) to 391 nm (TA-reacted fluorescamine) and the appearance of a fluorescence emission peak (ΔS) at 483 nm for the TA-fluorescamine reaction products corroborated the formation of the fluorophore. The TA standard solution yielded a linear concentration-fluorescence emission intensity curve, with a mean R^2 of 0.996 (N = 10).

Addition of 1% TX100 to the TA-fluorescamine reaction mixture slightly increased the amplitude of the fluorescence emission curve (λ_{range} = 415–675 nm) but did not affect the peak position (λ = 483 nm) or the linearity of the TA concentration-fluorescence emission intensity relationship (not shown). Incubation of TA and fluorescamine with TX100 for 24 h at RT, 4 °C, and −20 °C slightly affected the slope of the curve but not the linearity (Fig. 3(C)). Moreover, 24-h incubation at any temperature yielded higher fluorescence emission intensities relative to 30-min incubation, indicating that the reaction products remain stable for at least one day regardless of storage temperature. Although 24-h incubation at RT constituted the optimal reaction condition as evidenced by the relatively steep slope coefficient, linear regression analysis evinced that the other reaction conditions are equally suitable for the determination of TA concentration in detergent-treated buffered solutions (R^2 > 0.9926).

Author Manuscript Author Manuscript Author Manuscript Author Manuscript

To quantify liposomal TA, liposome-containing eluents had to be diluted 1,250× (total dilution factor, including the reaction mixture) in order for the TA concentration to fall in the range of the standard curve (0–4 μM TA).

Drug:Lipid Ratios, LUVET Sizes, and Polydispersities

TA was encapsulated in LUVETs composed of DPPC (control), DPPC with increasing concentrations DSPE-PEG (2, 4, and 6 mol%), DPPC containing 10 mol% MPPC, and DPPC containing 6 mol% DSPE-PEG and 10 mol% MPPC. MPPC was incorporated into conventional thermosensitive formulations due to its ability to speed up release kinetics during phase transition.[47] The formulations were assayed for TA:lipid ratio, vesicle size, and the extent of size homogeneity (polydispersity).

The post-gelfiltration TA:lipid ratios were 0.53–1.40% of the pre-gelfiltration TA:lipid ratios, which is ascribable to the removal of unencapsulated TA by size exclusion chromatography. Drug:lipid ratios can be used to deduce other outcome parameters (e.g., C_{TA}, L, and C_{lip}) in addition to providing insightful information when multiple formulations prepared in the same manner are juxtaposed. Notwithstanding the finding that the addition of PEG-conjugated DSPE at 2 and 4 mol% raised the TA:lipid ratio to respectively 0.89 (**) and 0.82 (*) versus control (TA:lipid ratio of 0.63), increasing concentrations of DSPE-PEG imposed a deleterious effect on the mean TA:lipid ratio (Fig. 4(A), formulations 2–4). DSPE-PEG concentrations of 6 mol% reduced the mean TA:lipid ratio by 16% (*) (Fig. 4(A), formulation 4 vs. 1). Similarly, incorporation of 10 mol% MPPC into unPEGylated DPPC LUVETs was associated with a mean decrease of 30% (*) (Fig. 4(A), formulation 5 vs. 1), whereas the reduction was 46% (**) for DPPC:MPPC LUVETs containing 6 mol% DSPE-PEG (Fig. 4(A), formulation 6) relative to control.

Another relevant parameter is LUVET size, which should remain within a specific range (~0.16–0.21 μm) for effective evasion of cells of the mononuclear phagocyte system (MPS) after systemic administration.[48] Liposomal formulations should therefore possess physicochemical properties that preclude aggregation/fusion. PCS revealed the sterically stabilizing effect of PEG, insofar as PEGylation deterred LUVET fusion and/or aggregation in buffer during storage. The mean±SD vesicle size of extruded unPEGylated DPPC formulations was 1,052 ± 180 nm (>5× greater than the filter pore size) with a mean polydispersity of 1.000 (result not shown), an effect that is consistent with previous reports.[49] Changes in polydispersity occurred within a few hours of storage at 4 °C. In contrast, the mean sizes of the PEGylated LUVETs (Fig. 4(B), formulations 2–4), which did not differ statistically from each other ($p \geq 0.212$), fell in the range of 152 to 166 nm with polydispersities of <0.091. MPPC-containing formulations (Fig. 4(B), formulations 5, 6) exhibited similar characteristics. Interestingly, aggregation/fusion did not occur when MPPC was incorporated into unPEGylated DPPC LUVETs (Fig. 4(B), formulation 5).

The results corroborate the importance of PEGylation but concomitantly underscore the balance that has to be struck between the level of ‘stealth’ imposed on the formulation and endovesicular drug concentration, since these are apparently governed by an inversely proportional relationship. The incorporation of MPPC further undermined this balance.

Author Manuscript Author Manuscript Author Manuscript Author Manuscript

Accordingly, DPPC:DSPE-PEG (96:4) is the most suitable formulation for antifibrinolytic SSPLT based on the combination of TA:lipid ratio, size, and degree of steric stabilization.[50]

Encapsulation Efficiencies (E_{eff}), Trapped Volumes (V_t), and Endovesicular TA Concentrations (C_{TA})

Table II presents the E_{eff}, V_t, and C_{TA} of the formulations based on the experimentally obtained TA:lipid ratios and vesicle sizes, phospholipid molecular areas derived from literature, and the computed values summarized in Table III. Since these outcome parameters are predominantly dependent on the former, the trends in E_{eff}, V_t, and C_{TA} conform to the trends exhibited by the TA:lipid ratios and LUVET sizes (Fig. 4).

The E_{eff} is a derivative of the drug:lipid ratio and is useful for relative interpretations as indicated above. A strong negative correlation existed between the E_{eff} and extent of PEGylation (Pearson's $r = -0.915$**), which, in relation to a uniform LUVET size distribution across the MPPC-lacking PEGylated formulations and the absence of a correlation between E_{eff} and size ($r = -0.244$, N.S.), implies a volumetric occupation by the PEG chains in the LUVET aqueous compartment (Table II, formulations 2–4). The inclusion of MPPC further reduced the E_{eff} and caused a greater decrease in this parameter in conjunction with 6 mol% DSPE-PEG (Table II, formulations 5 and 6, respectively, vs. 1, corresponding to reductions in E_{eff} of 29% and 46%, respectively).

The V_ts were determined numerically based on the particle size data obtained by PCS, assuming a spherical morphology. The V_ts of the formulations (Table II) fell in the range as reported in literature for comparable formulations,[34, 51] notwithstanding differences in DPPC areas (A) and the potential 20–40% volume overestimation as a result of morphology-related assumptions.[35, 51]

The C_{TA}, calculated on the basis of particle size, phospholipid area, and TA:lipid ratio, is a crucial parameter in relation to active release rates and targeting efficacy inasmuch as it ultimately determines the clinical dosage. The C_{TA} should be maximized within physiological confines such as osmolarity and toxicity so that an optimal (local) drug concentration can be achieved with a minimal amount of vehicle. All formulations exhibited a reduced C_{TA} that comprised 68%–30% of the initial 318 mM TA concentration in the hydration solution. This was likely a result of the spatial occupation by PEG and, to a limited extent, of possibly aberrant phospholipid areas used in the computations. Nevertheless, conclusions can be drawn from the relative differences inasmuch as these are, in this case, hardly impacted by model assumptions. Formulations 4–6 had a significantly (**) reduced C_{TA} compared to formulations 2 and 3 (Table II), implying that PEG concentrations >4 mol% and MPPC exerted a profound debilitating effect on the C_{TA}.

Taken altogether, DPPC:DSPE-PEG (96:4) remains the most suitable formulation for antifibrinolytic SSPLT given the negligible differences in E_{eff}, V_t, and C_{TA} between formulations 2 and 3.

Author Manuscript Author Manuscript Author Manuscript Author Manuscript

Heat-Induced Tranexamic Acid Release from Thermosensitive Liposomes in Buffer

Liposomes composed of phospholipids that have a T_m slightly above body temperature constitute ideal drug carriers for tissue targets that are easily accessible to artificially-induced hyperthermic conditions. Consequently, therapeutic agents loaded into thermosensitive liposomes can be actively released in a controlled fashion by heating the target site to T_m, which results in thermotropic alterations of the lipid bilayer and corollary increase in bilayer permeability and outward diffusion of encapsulated drugs.[26] To validate the hyperthermia model for two types of TA-encapsulating thermosensitive stealth formulations, TA-encapsulating DPPC:DSPE-PEG (96:4, T_m = 42.3 °C, Fig. 5(A)) and DPPC:MPPC:DSPE-PEG (86:10:4, T_m = 41.5 °C, Fig. 5(B)) LUVETs were heated at T_m and 4 °C below T_m and assayed for the percentage of TA release as a function of time.

The mean ± SD TA concentration in the supernatant of the centrifuge control samples of DPPC:DSPE-PEG (96:4) and DPPC:MPPC:DSPE-PEG (86:10:4) LUVETs was 2.4±5.1% (N = 48) and 7.1±11.1% (N = 56) of the total vesicular TA concentration, respectively. The heating of DPPC:DSPE-PEG (96:4) LUVETs to phase transition caused a rapid release of TA that proceeded in a sigmoidal pattern (Fig. 5(C)). The most substantial release occurred between 0.5 and 2.5 min, corresponding to a mean release of 2.4% and 95.5%, respectively, and a mean release rate of 0.78%·s^{-1}. Moreover, TA release occurred at a very high release capacity (the maximum amount of drug released), approximating 100% within 2.5 min. Elevation of the temperature to 39.3 °C (control) also induced drug release, but at a much slower rate, accounting for a release of ~13% after 5 min (Fig. 5(C)). This may have been due to the broader left transition shoulder as seen in the DPPC:DSPE-PEG thermogram (Fig. 5(A)), which entails the control temperature. The incorporation of 10 mol% MPPC sped up the release kinetics, whereby the most rapid drug release occurred between 0.5 (2.1%) and 2.0 min (93.0%), corresponding to a mean release rate of 1.02%·s^{-1} (Fig. 5(D)). Heating the formulation to 36.0 °C resulted in negligible diffusion of TA from the LUVETs.

In light of the fast release kinetics and the high release capacity of the conventional thermosensitive formulation and the substantially reduced E_{eff} and C_{TA} of MPPC-containing LUVETs, the incorporation of MPPC yielded no surpassing advantages to advocate its potential applicability in the antifibrinolytic component of SSPLT.

Interpolated *In Vivo* Posologies

Following characterization of the LUVETs and determination of heat-induced drug release profiles, a model was developed to interpolate the number of TA-encapsulating LUVETs and final lipid concentrations required for an optimal antifibrinolytic effect in 500-μm long vessel segments of diameters that are representative for PWS vasculature. Final TA concentrations were predicated on clinically prescribed dosages, producing L_m (number of minimally required LUVETs) ranges in the order of 10^6–10^8 for 30–200-μm vessel diameters, respectively (Figs. 6(A, B)). The C_{lip} (lipid concentration) values comprised 2.1, 2.7, and 4.3 mM for DPPC:DSPE-PEG LUVETs with 98:2, 96:4, and 94:6 molar ratios, respectively, and 5.6 and 8.0 mM for DPPC:MPPC (90:10) and DPPC:MPPC:DSPE-PEG (86:10:4) LUVETs respectively.

Author Manuscript Author Manuscript Author Manuscript Author Manuscript

Computational analysis was subsequently performed on a 3D histological reconstruction of a PWS (Fig. 6(B)) to derive the dermal blood volume, which yielded 2.15 μL blood per cm^2 skin surface. With a target TA concentration of 1.9 mM and an approximated quantity of TA molecules per vesicle (Q_{TA}) for each formulation, the L_{PWS} could be interpolated for PWS of different surface areas (A_{PWS}) as presented in Figure 6(C). For A_{PWS} between 5 and 40 cm^2, the L_{PWS} ranged from 41–327 for DPPC:DSPE-PEG (98:2) at the lower end and from 156–1,247 for DPPC:MPPC:DSPE-PEG2000 (86:10:4) at the upper end, respectively.

LUVET Association with Hamster and Human Platelets

In light of the beneficial physicochemical properties and release kinetics of the *F3* LUVETs, the following series of experiments were conducted to determine LUVET toxicity and pharmacokinetics. In the first set of experiments, the association between *F3* CF-LUVETs and resting and activated isolated hamster and human platelets was determined by flow cytometry, given that blood cells constitute the first point of contact following systemic administration. The flow cytograms were analyzed for mean CF fluorescence intensity (indicative of LUVET-platelet association/uptake) and the percentage of upper right quadrant cells (indicative of the extent of the LUVET-platelet association). The data is presented in Table IV and representative flow cytograms are provided in Figure 7. The *F3* CF-LUVETs used in these and the *ex vivo* RBC experiments (Section LUVET Association with Red Blood Cells) had a mean±SD diameter of 116.0 ± 5.6 nm, a PDI of 0.338 ± 0.010, and a ζ-potential of −1.6±3.2 mV.

Resting and activated hamster and human platelets exhibit weak autofluorescence. Incubation of resting and activated hamster and human platelets with *F3* CF-LUVETs and immediate washing of the platelets resulted in an increase in fluorescence intensity compared to the autofluorescence control, suggesting LUVET-platelet association/uptake. The 30-min incubation before washing did not alter the fluorescence emission intensity, indicating that the association/uptake is very rapid.

However, the mean intensity of the fluorescence from platelets (range of 3.6–5.8 a.u., Table IV) did not correspond to the mean FL1 fluorescence intensity of single LUVETs (191.3 a.u., Table IV and Fig. 8). Accordingly, either the LUVETs had been taken up by the platelets[52] and the CF fluorescence was quenched by intracellular proteins as reported for plasma in Heger et al.[32] or the CF had leaked out of the LUVETs during incubation (Fig. 9) and was internalized by the platelets.[32] The latter seems more likely given that, firstly, similar CF-LUVETs composed of mainly DSPC ($T_m \approx 54$ °C)[53] did not leak CF[32] in comparable experiments and did not exhibit notable LUVET-platelet interactions *in vitro*[54] or *in vivo*.[32] Secondly, cell-particle interactions are mainly governed by the particle's composition, surface charge, and size,[55] which were essentially the same between the stable DSPC LUVETs[32] and the *F3* LUVETs used in this study. The exact nature of the *F3* LUVET-platelet interactions/uptake, if any, will be investigated in more detail in a separate study, but at this point there is no unequivocal evidence to conclude that *F3* LUVETs interact with or are taken up by resting or activated platelets.

Author Manuscript Author Manuscript Author Manuscript Author Manuscript

LUVET Association with Red Blood Cells

Next, similar *in vitro* experiments were performed with isolated human and hamster RBCs, of which the data are provided in Table V and exemplary flow cytograms are shown in Figure 10. The RBCs that had been washed immediately after addition of *F3* CF-LUVETs fluoresced more intensely than isolated RBCs (autofluorescence control), albeit significantly less than the mean fluorescence intensity of single liposomes (Table V and Fig. 8). The 30-min incubation step did not yield a noteworthy increase in fluorescence intensity, indicating that no addition association/uptake had occurred. Just as with the platelets, the positive staining may have emanated from the uptake of leaked CF from the LUVETs (Fig. 10), which was confirmed in separate experiments with isolated RBCs for CF but also the more anionic fluorescein derivative calcein (Fig. 11).

Conversely, the *in vivo* experiments, which were performed with a covalently attached fluorescent label (NBD-PC) to preclude fluorophore leakage, suggest that liposomes did in fact associate with RBCs. The NBD-LUVETs used in these experiments had a mean ± SD diameter of 100.3±2.1 nm and a PDI of 0.165±0.130. The association/uptake was most profound after 15 min of circulation and abated at 45 min circulation. However, the fluorescence intensity of the RBCs was almost two orders of magnitude lower than that of single LUVETs (Fig. 12). This is somewhat elusive inasmuch as cell-bound or internalized fluorescent particles should theoretically confer the same fluorescence intensity of the fluorescent particle to the cell when assayed by flow cytometry. It is known, however, that C_6-NBD-PC can be transferred from LUVETs to acceptor membranes, including those of RBCs, by lipid binding proteins present in blood, such as albumin.[56] As with the platelets, the association/uptake kinetics will be investigated more closely in an ensuing study.

In light of the possible association/uptake of the LUVETs by RBCs, hemolysis studies were performed with empty LUVETs, TA-encapsulating LUVETs, and free TA to ensure that the particles or drug do not perturb the structural integrity of RBCs following association/uptake. As shown in Figure 13, neither formulation nor TA induced any notable hemolysis up to a final lipid concentration of 1 mM or final TA concentration of 100 μM during 3 h at 37 °C.

Uptake and Toxicity of *F*3 LUVETs in Cultured Cells

In addition to platelets and RBCs, systemically infused LUVETs also come in contact with endothelial cells lining the blood vessels, circulating and stationary leukocytes that clear the particles from the circulation, and the liver, which takes up, detoxifies, and eliminates xenobiotics from the blood.[57] Accordingly, uptake of the *F3* TA-LUVETs by these cells may confer cytotoxicity, both of which were tested in the last set of experiments in cultured HUVECs, RAW 264.7 macrophages, and HepG2 hepatocytes.

As shown in Figure 14, the uptake of fluorescently labeled *F3* LUVETs (mean ± SD diameter of 166.0 ± 2.0 nm and a PDI of 0.074 ± 0.027) was absent in HUVECs, mild in hepatocytes, and profound in macrophages up to a final lipid concentration of 1 mM. The degree of uptake of cationic liposomes (mean ± SD diameter of 191.5± 1.1 nm and a PDI of 0.077± 0.042), which were used as positive control, was considerably higher in HUVECs

Author Manuscript Author Manuscript Author Manuscript Author Manuscript

and hepatocytes compared to *F3* LUVETs but approximately equal in macrophages. The uptake of cationic liposomes proceeded in the order HUVECs < RAW 264.7 macrophages ≈ HepG2 hepatocytes. Moreover, the results obtained with the cationic liposomes de facto argue against the transfer of NBD-PC from the LUVETs to the cells by lipid binding proteins (i.e., FCS), as alluded to earlier.

The absence of LUVET uptake by HUVECs essentially translated to unaffected mitochondrial redox states (WST-1) and cell viability (SRB) following incubation with empty (mean±SD diameter of 178.5±0.6 nm and a PDI of 0.042±0.035, after size exclusion chromatography) or TA-encapsulating *F3* LUVETs (mean±SD diameter of 176.7 ± 1.3 nm and a PDI of 0.041 ± 0.047, after size exclusion chromatography) (Fig. 14) up to a 400-μM final lipid concentration. The reduction of WST-1 to its formazan chromophore form became slightly perturbed at the highest lipid concentrations, but did not result in exacerbation of cell death. Unencapsulated TA was not toxic to HUVECs. In contrast, the considerable uptake of *F3* LUVETs by RAW 264.7 macrophages resulted in a moderately impaired mitochondrial redox state and considerably reduced cell viability in a phospholipid- and TA concentration-dependent manner. This effect was solely attributable to TA but not the lipids, given that empty LUVETs imparted no effect on either outcome parameter (Fig. 14). Lastly, hepatocytes were not affected by any of the constituents despite moderate uptake of LUVETs (Fig. 14).

DISCUSSION

Selective photothermolysis, or the selective destruction of blood vessels by pulsed laser irradiation, was introduced in 1983 as a means to non-invasively remove aberrant cutaneous vasculature through controllable photothermal processes.[8] Presently, selective photothermolysis represents the gold standard treatment of PWS (capillary malformations), with extended applicability in dermatology and ophthalmology.[58] Although PWS can be effectively treated by selective photothermolysis, there are several inevitable intrinsic factors, including epidermal pigmentation,[59] optical shielding by blood and superimposed vessels,[17, 19, 60] and PWS anatomy and morphology,[18, 61, 62] that are responsible for suboptimal outcomes in approximately 60% of patients.[19, 63] Inasmuch as these factors are difficult to circumvent completely by external means (e.g., by using different laser parameters or dynamic cooling),[61–64] SSPLT was devised to tackle poor lesional clearance rates from within the vasculature.

As presented in the caption of Figure 1, SSPLT entails a prothrombotic component and an antifibrinolytic component. In an effort to develop an antifibrinolytic drug delivery platform for SSPLT, a liposomal system was selected for the encapsulation of TA, a potent antifibrinolytic agent used in the clinical setting to inhibit plasmin-mediated thrombolysis. Inasmuch as SSPLT relies on the laser-induced generation of heat, the rudimentary design of liposomes was based on thermosensitivity as the main drug release mechanism. Hence, TA-encapsulating DPPC(:MPPC) and DPPC(:MPPC):DSPE-PEG formulations were assayed for TA:lipid ratio and size so as to derive E_{eff}, V_{t}, and C_{TA}, after which heat-induced TA release was quantified for the most optimal candidate formulation in the absence and presence of

Author Manuscript Author Manuscript Author Manuscript Author Manuscript

lysolipid. In the final analysis, *F3* LUVETs composed of DPPC:DSPE-PEG in a 96:4 molar ratio were the most suitable formulation for antifibrinolytic SSPLT.

The most relevant parameters regarding DPPC:DSPE-PEG (96:4) LUVETs in light of the further development of SSPLT as a clinical modality include the TA:lipid ratio, E_{eff}, C_{TA}, and the release kinetics inasmuch as these chiefly dictate posology. At a mean TA:lipid ratio of 0.82 and an E_{eff} of 1.29%, the prime candidate formulation encompassed a C_{TA} of 214 mM and a release rate of approximately 100% in 2.5 min. Notwithstanding differences in liposome composition, the TA:lipid ratio of DPPC:DSPE-PEG LUVETs was comparable to or higher than drug:lipid ratios reported for liposome-encapsulated anti-cancer drugs such as doxorubucin,[65] paclitaxel,[66] and N_3-*O*-toluyl-5-fluorouracyl.[67] In contrast, the E_{eff} was substantially lower than most of these compounds, which is the result of the relatively high initial TA:lipid ratio (63.6) and the excessive removal of unencapsulated TA during size exclusion chromatography in combination with the preparation technique (hydration of lipid film).

An unexpected finding was that heat-induced TA release from the candidate formulation occurred at an exceptionally fast rate and at a ~100% release capacity. David Needham's group reported release times and release capacities in the order of ~5 min and ~85% release of carboxyfluorescein from lysolecithin (MPPC)-containing thermosensitive liposomes, respectively, ~20 min and ~40% release of doxorubicin from traditional thermosensitive liposomes (comparable to *F3* LUVETs), respectively, and ~5 min and ~50% release of doxorubicin from MPPC-containing thermosensitive liposomes, respectively.[26] A marked contribution of MPPC to the release kinetics, as has been reported previously,[26, 47] was absent with respect to TA-encapsulating *F3* LUVETs. Although the exact reasons for these substantial differences were not investigated, the small size of TA may contribute to a less constrained passage through the laterally decompressed membrane during phase transition—a phenomenon that is accompanied by increased membrane hydration state,[68] corollary packing defects and cavitation,[69] and a lowered transmembrane free energy barrier,[70, 71] all of which actuate a greater extent of diffusion of ions and higher molecular weight compounds such as doxorubicin and carboxyfluorescein versus gel phase or liquid crystalline states. It is expected that, under these conditions, smaller molecules (e.g., TA) transgress the membrane more facilely than larger ones (e.g., carboxyfluorescein and doxorubicin).

The release kinetics of *F3* LUVETs are, within the limits of the *in vitro* data, ideal in the context of selective photothermolysis-related endovascular laser-tissue interactions.[10] The hemodynamic response (thrombosis), that occurs in consequence to the photothermal response (laser-induced thermal coagulum formation), is characterized by a growth phase and a deterioration phase.[15] The hemostatic equilibrium shifts to a predominantly prothrombotic state during the growth phase and to a predominantly fibrinolytic state during the deterioration phase. Using a hamster dorsal skin fold model in combination with laser-mediated endovascular damage induction,[14, 15] we demonstrated that the prothrombotic state reaches a maximum at approximately 6.25 min following laser irradiation.[14] In order to extend this state through the inhibition of fibrinolysis, accumulation of the drug carrier is exacted during the early formative stages of the thrombus so that TA-encapsulating

Author Manuscript Author Manuscript Author Manuscript Author Manuscript

liposomes can progressively accumulate into the developing clot concomitantly with plasminogen,[72] particularly in venules,[73] and its agonist tissue plasminogen activator (tPA).[24] Theoretically, this should be possible given the rapid release kinetics of the *F3* LUVETs compared to the 2.5-fold longer duration of the growth phase, allowing TA to first accumulate at the target site and then be released into the clot before (and during) the transition to a fibrinolytic state. Furthermore, the high release capacity of this formulation is considerably advantageous since about three LUVETs are required to completely inhibit plasminogen bound to one activated platelet, taking into account a saturation level of $1.9\pm0.5 \times 10^5$ plasminogen molecules per platelet,[72] 5 lysine binding sites per plasminogen molecule,[74] and the encapsulation of roughly 3×10^5 TA molecules per LUVET (Table III).

Secondly, the favorable release kinetics and release capacity of *F3* LUVETs enforce the potential applicability of the envisaged SSPLT regimen in a clinical setting. The therapeutic procedures may be performed on an outpatient basis, whereby the LUVET formulation would be systemically administered 10–15 min before laser treatment to ensure homogenous distribution throughout the circulation. Subsequently, a lasing regime would be performed on the PWS to induce the hemodynamic response, after which the irradiated region is selectively heated, e.g., by a heating pad or near infrared light, to trigger drug release so as to facilitate complete blockage of the semi-coagulated vasculature. Since this has to occur within the time span of the hemodynamic response, the total duration of the actual procedure will be determined chiefly by the number of lasing/heating cycles needed to treat the entire PWS, which in turn depends on the size of the lesion. The majority of PWS is <40 cm^2 in size,[75] which eliminates the need for excessively long treatment sessions.

In terms of pharmacokinetics and toxicity, the (TA-encapsulating) *F3* LUVETs also exhibited a relatively favorable profile. Upon infusion, liposomes come in contact with circulating blood cells (platelets, RBCs, leukocytes), endothelial cells, and phagocytic cell-containing organs such as the liver and spleen. The *F3* LUVETs did not associate with platelets (although at this point not unequivocally ruled out) and RBCs *ex vivo* and cultured HUVECs and hepatocytes. Accordingly, little-to-no toxicity was observed in the latter three cell types. The *F3* LUVETs did associate with RBCs *in vivo* but without inducing hemolysis, so the only possible implication is that RBC-associated LUVETs may not incorporate into laser-induced thrombi, which needs to be further investigated in subsequent studies. Given that so few thrombus-incorporated LUVETs are necessary to deter fibrinolysis following heat-induced TA release, the LUVET-RBC interactions are not expected to be deleterious to SSPLT. The greatest potential concern is the uptake by and toxicity in RAW 264.7 macrophages, which are analogous to circulating leukocytes and liver-resident Kupffer cells. The administration of TA-encapsulating *F3* LUVETs may temporarily impair innate immunity due to TA-induced leukocyte depletion, albeit this must be confirmed in *in vivo* studies. On the other hand, TA has been used at relatively high concentrations in the clinical setting for years and toxicity profiles are well-established. Encapsulation of TA into liposomes did not seem to alter its pharmacodynamics in terms of cytotoxicity, so the consequences regarding *in vivo* cytotoxicity are not expected to be serious until further studies prove otherwise.

Author Manuscript Author Manuscript Author Manuscript Author Manuscript

In conclusion, several rudimentary liposomal formulations were explored for the antifibrinolytic component of SSPLT, and their properties and heat-induced release profiles juxtaposed to selective photothermolysis-related endovascular laser-tissue interactions and criteria for clinical application. Although several features will have to be optimized and/or added (e.g., targeting), *F3* LUVETs evolved as the prime candidate formulation. In light of forthcoming *in vivo* research, models were developed to facilitate LUVET accumulation and release experiments in singular vessels such as previously published or to further assess posology based on PWS dimensions.[13–15] In case of the former, assays could be set up by using fluorescently-labeled LUVETs and correlating the emitted fluorescence from accumulated LUVETs in laser-induced thrombi to a lipid or LUVET concentration. Subsequently, heat-induced TA release from the accumulated LUVETs could be quantified from blood as previously described.[25] The mathematical approximations and computational models presented here will also be useful in current and future research aimed at vehicular targeting, including thermosensitive immunoLUVETs that recognize specific epitopes on activated platelets or fibrin, and the prothrombotic component of SSPLT. Further studies will also be performed in animal models to establish proof-of-principle and assess pharmacokinetics and disposition of TA-containing *F3* LUVETs.

Acknowledgments

Michal Heger was supported by Stichting Technologische Wetenschap, the Nijbakker-Morra Foundation, an SKE preseed grant from the Academic Medical Center, and a personal grant from Novo Nordisk. Anton I. de Kroon received financial support from NanoNed. Bernard Choi was supported by the Arnold and Mabel Beckman Foundation and the U.S. National Institutes of Health (R01 HD065536). The LUVET-RBC interaction experiments were performed at the Catholic University of Leuven at Kortrijk, Belgium, in the laboratory of professor Hans Deckmyn. We are grateful to Isabelle Salles for assistance with the flow cytometry experiments and the volunteers for donating blood. We thank Martha van Herwaarden for assistance with the osmometer and Joan Kwakkel for providing the RAW 264.7 cells. Albert van Wijk is acknowledged for help with the HUVEC isolation from umbilical cords. Finally, we thank Joost Huiskens for the blood drawing, Marjorie Rosheuvel and the Clinical Chemistry Department for the blood cell counting, and Thomas van Gulik for facilitating lab space.

References

1. Klapman MH, Yao JF. Thickening and nodules in port-wine stains. J Am Acad Dermatol. 2001; 44:300. [PubMed: 11174392]
2. Barsky SH, Rosen S, Geer DE, Noe JM. The nature and evolution of port wine stains: A computer-assisted study. J Invest Dermatol. 1980; 74:154. [PubMed: 7359006]
3. Lanigan SWW, Cotterill JAA. Psychological disabilities amongst patients with port wine stains. Br J Dermatol. 1989; 121:209. [PubMed: 2775645]
4. Malm M, Carlberg M. Port-wine stain-a surgical and psychological problem. Ann Plast Surg. 1988; 20:512. [PubMed: 3389703]
5. Tallman B, Tan OT, Trainor S. Location of port-wine stains and the likelihood of ophthalmic and/or central nervous system complications. Pediatrics. 1991; 87:323. [PubMed: 1805804]
6. Hennedige AA, Quaba AA, Al-Nakib K. Sturge-weber syndrome and dermatomal facial port-wine stains: Incidence, association with glaucoma, and pulsed tunable dye laser treatment effectiveness. Plast Reconstr Surg. 2008; 121:1173. [PubMed: 18349634]
7. Comi AM. Topical review: Pathophysiology of sturge-weber syndrome. J Child Neurol. 2003; 18:509. [PubMed: 13677575]
8. Anderson RR, Parrish JA. Selective photothermolysis: Precise microsurgery by selective absorption of pulsed radiation. Science. 1983; 220:524. [PubMed: 6836297]

Author Manuscript Author Manuscript Author Manuscript Author Manuscript

9. Chen JKJK, Ghasri P, Aguilar G, van Drooge AM, Wolkerstorfer A, Kelly KM, Heger M. An overview of clinical and experimental treatment modalities for port wine stains. J Am Acad Dermatol. 2012; 67:289. [PubMed: 22305042]
10. Heger M, Beek JF, Moldovan NI, van der Horst C, van Gemert MJC. Towards optimization of selective photothermolysis: Prothrombotic pharmaceutical agents as potential adjuvants in laser treatment of port wine stains. A theoretical study. Thromb Haemost. 2005; 93:242. [PubMed: 15711739]
11. Heger M, Bezemer R, Huertas-Pérez JF, Dekker H, Beek JF. Endovascular laser-tissue interactions redefined: Shining light on novel windows of therapeutic opportunity beyond selective photothermolysis. Photomed Laser Surg. 2010; 28:569. [PubMed: 20704498]
12. Aguilar G, Choi B, Broekgaarden M, Yang O, Yang B, Ghasri P, Chen JK, Bezemer R, Nelson JS, van Drooge AM, Wolkerstorfer A, Kelly KM, Heger M. An overview of three promising mechanical, optical, and biochemical engineering approaches to improve selective photothermolysis of refractory port wine stains. Ann Biomed Eng. 2012; 40:486. [PubMed: 22016324]
13. Heger M, Beek J, Stenback K, Faber D, van Gemert M, Ince C. Darkfield orthogonal polarized spectral imaging for studying endovascular laser-tissue interactions *in vivo*—A preliminary study. Opt Express. 2005; 13:702. [PubMed: 19494931]
14. Bezemer R, Heger M, van den Wijngaard JPH, Mordon SR, van Gemert MJC, Beek JF. Laser-induced (endo)vascular photothermal effects studied by combined brightfield and fluorescence microscopy in hamster dorsal skin fold venules. Opt Express. 2007; 15:8493. [PubMed: 19547183]
15. Heger M, Salles II, Bezemer R, Cloos MA, Mordon SR, Bégu S, Deckmyn H, Beek JF. Laser-induced primary and secondary hemostasis dynamics and mechanisms in relation to selective photothermolysis of port wine stains. J Dermatol Sci. 2011; 63:139. [PubMed: 21664109]
16. Heger M, van Golen RF, Broekgaarden M, van den Bos RR, Neumann HAM, van Gulik TM, van Gemert MJC. Endovascular laser–tissue interactions and biological responses in relation to endovenous laser therapy. Lasers Med Sci. 2014; 29:405. [PubMed: 24232911]
17. Fiskerstrand EJ, Svaasand LO, Kopstad G, Ryggen K, Aase S. Photothermally induced vessel-wall necrosis after pulsed dye laser treatment: Lack of response in port-wine stains with small sized or deeply located vessels. J Invest Dermatol. 1996; 107:671. [PubMed: 8875947]
18. Fiskerstrand EJ, Svaasand LO, Kopstad G, Dalaker M, Norvang LT, Volden G. Laser treatment of port wine stains: Therapeutic outcome in relation to morphological parameters. Br J Dermatol. 1996; 134:1039. [PubMed: 8763421]
19. Hohenleutner U, Hilbert M, Wlotzke U, Landthaler M. Epidermal damage and limited coagulation depth with the flashlamp-pumped pulsed dye laser: A histochemical study. J Invest Dermatol. 1995; 104:798. [PubMed: 7738359]
20. Levy JH. Pharmacologic preservation of the hemostatic system during cardiac surgery. Ann Thorac Surg. 2001; 72:S1814. [PubMed: 11722115]
21. Karski J, Djaiani G, Carroll J, Iwanochko M, Seneviratne P, Liu P, Kucharczyk W, Fedorko L, David T, Cheng D. Tranexamic acid and early saphenous vein graft patency in conventional coronary artery bypass graft surgery: A prospective randomized controlled clinical trial. J Thorac Cardiovasc Surg. 2005; 130:309. [PubMed: 16077392]
22. Mannucci PM. Treatment of von Willebrand disease. Thromb Haemost. 2001; 86:149. [PubMed: 11487002]
23. Hoylaerts M, Lijnen HR, Collen D. Studies on the mechanism of the antifibrinolytic action of tranexamic acid. Biochim Biophys Acta. 1981; 673:75. [PubMed: 7193484]
24. Medved L, Nieuwenhuizen W. Molecular mechanisms of initiation of fibrinolysis by fibrin. Thromb Haemost. 2003; 89:409. [PubMed: 12624622]
25. Huertas-Pérez JF, Heger M, Dekker H, Krabbe H, Lankelma J, Ariese F. Simple, rapid, and sensitive liquid chromatography-fluorescence method for the quantification of tranexamic acid in blood. J Chromatogr A. 2007; 1157:142. [PubMed: 17532325]
26. Needham D, Dewhirst MW. The development and testing of a new temperature-sensitive drug delivery system for the treatment of solid tumors. Adv Drug Del Rev. 2001; 53:285.

Author Manuscript Author Manuscript Author Manuscript Author Manuscript

27. Maruyama K, Unezaki S, Takahashi N, Iwatsuru M. Enhanced delivery of doxorubicin to tumor by long-circulating thermosensitive liposomes and local hyperthermia. Biochim Biophys Acta. 1993; 1149:209. [PubMed: 8323940]
28. Gaber MH, Wu NZ, Hong K. Thermosensitive liposomes: Extravasation and release of contents in tumor microvascular networks. Int J Radiat Oncol Biol Phys. 1996; 36:1177. [PubMed: 8985041]
29. Heger, M. Drug delivery system for use in the treatment of vascular and vessel-related pathologies. US Patent. 20120010557. Jan 12. 2012
30. Rouser G, Fleischer S, Yamamoto A. Two dimensional thin layer chromatographic separation of polar lipids and determination of phospholipids by phosphorus analysis of spots. Lipids. 1970; 5:494. [PubMed: 5483450]
31. Broekgaarden M, de Kroon AIPM, Gulik TMV, Heger M. Development and *in vitro* proof-of-concept of interstitially targeted zinc-phthalocyanine liposomes for photodynamic therapy. Curr Med Chem. 2013; 21:377.
32. Heger M, Salles II, van Vuure W, Hamelers IHL, de Kroon AIPM, Deckmyn H, Beek JF. On the interaction of fluorophore-encapsulating PEGylated lecithin liposomes with hamster and human platelets. Microvasc Res. 2009; 78:57. [PubMed: 19281828]
33. Udenfriend S, Stein S, Böhlen P, Dairman W, Leimgruber W, Weigele M. Fluorescamine: A reagent for assay of amino acids, peptides, proteins, and primary amines in the picomole range. Science. 1972; 178:871. [PubMed: 5085985]
34. Zuidam, NJ., de Vrueh, R., Crommelin, DJ. Liposomes: A Practical Approach. Torchilin, VP., Weissig, V., editors. Oxford University Press; Oxford: 2003. p. 64
35. Nagle JF, Tristram-Nagle S. Lipid bilayer structure. Curr Opin Struct Biol. 2000; 10:474. [PubMed: 10981638]
36. Majewski J, Kuhl TL. X-ray synchrotron study of packing and protrusions of polymer-lipid monolayers at the air-water interface. J Am Chem Soc. 1998; 7863:1469.
37. Chi LM, Wu WG. Effective bilayer expansion and erythrocyte shape change induced by monopalmitoyl phosphatidylcholine quantitive light microscopy and nuclear magnetic resonance spectroscopy measurements. Biophys J. 1990; 57:1225. [PubMed: 2393706]
38. Tahara Y, Fujiyoshi Y. A new method to measure bilayer thickness: Cryo-electron microscopy of frozen hydrated liposomes and image simulation. Micron. 1994; 25:141. [PubMed: 8055245]
39. Smithies DJ, van Gemert MJ, Hansen MK, Milner TE, Nelson JS. Three-dimensional reconstruction of port wine stain vascular anatomy from serial histological sections. Phys Med Biol. 1997; 42:1843. [PubMed: 9308088]
40. Upson C, Faulhaber T, Laidlaw D, Schlcgel D, Gurwitz R, Dam AV. Scientific visualization the application visualization system: A computational environment for scientific visualization. IEEE Comput Graph Appl. 1989; 9:30.
41. Selim MM, Kelly KM, Nelson JS, Wendelschafer-Crabb G, Kennedy WR, Zelickson BD. Confocal microscopy study of nerves and blood vessels in untreated and treated port wine stains: Preliminary observations. Dermatol Surg. 2004; 30:892. [PubMed: 15171768]
42. Chauhan S, Gharde P, Bisoi A, Kale S, Kiran U. A comparison of aminocaproic acid and tranexamic acid in adult cardiac surgery. Ann Card Anaesth. 2004; 7:40. [PubMed: 17827560]
43. Cauwenberghs N, Vanhoorelbeke K, Vauterin S, Westra DF, Romo G, Huizinga EG, Lopez JA, Berndt MC, Harsfalvi J, Deckmyn H. Epitope mapping of inhibitory antibodies against platelet glycoprotein Ibalpha reveals interaction between the leucine-rich repeat N-terminal and C-terminal flanking domains of glycoprotein Ibalpha. Blood. 2001; 98:652. [PubMed: 11468163]
44. Durán-Lara E, Guzmán L, John A, Fuentes E, Alarcón M, Palomo I, Santos LS. PAMAM dendrimer derivatives as a potential drug for antithrombotic therapy. Eur J Med Chem. 2013; 69:601. [PubMed: 24095753]
45. Post ICJH, de Boon WMI, Heger M, van Wijk ACWA, Kroon J, van Buul JD, van Gulik TM. Endothelial cell preservation at hypothermic to normothermic conditions using clinical and experimental organ preservation solutions. Exp Cell Res. 2013; 319:2501. [PubMed: 23792081]
46. Vichai V, Kirtikara K. Sulforhodamine B colorimetric assay for cytotoxicity screening. Nat Protoc. 2006; 1:1112. [PubMed: 17406391]

Author Manuscript Author Manuscript Author Manuscript Author Manuscript

47. Anyarambhatla GR, Needham D. Enhancement of the phase transition permeability of DPPC liposomes by incorporation of MPPC: A new temperature-sensitive liposome for use with mild hyperthermia. J Liposome Res. 1999; 9:491.
48. Awasthi VD, Garcia D, Goins BA, Phillips WT. Circulation and biodistribution profiles of long-circulating PEG-liposomes of various sizes in rabbits. Int J Pharm. 2003; 253:121. [PubMed: 12593943]
49. Sriwongsitanont S, Ueno M. Effect of a PEG lipid (DSPE-PEG2000) and freeze-thawing process on phospholipid vesicle size and lamellarity. Colloid Polym Sci. 2004; 282:753.
50. Vermehren C, Jørgensen K, Frokjaer S. Influence of lipopolymer concentration on liposome degradation and blood clearance. Int J Pharm. 1999; 183:13. [PubMed: 10361145]
51. Huster D, Jin AJ, Arnold K, Gawrisch K. Water permeability of polyunsaturated lipid membranes measured by 17O NMR. Biophys J. 1997; 73:855. [PubMed: 9251802]
52. Heger M, Salles, Van Vuure W, Dechkmyn H, Beek JF. Fluorescent labeling of platelets with polyanionic fluorescein derivatives. Anal Quant Cytol Histol. 2009; 31:227. [PubMed: 19736870]
53. Kučerka N, Nieh MP, Katsaras J. Fluid phase lipid areas and bilayer thicknesses of commonly used phosphatidylcholines as a function of temperature. Biochim Biophys Acta. 2011; 1808:2761. [PubMed: 21819968]
54. Heger M, Salles II, de Kroon AIPM, Deckmyn H. Platelets and PEGylated lecithin liposomes: When stealth is allegedly picked up on the radar (and eaten). Microvasc Res. 2009; 78:1. [PubMed: 19306888]
55. Dan N. Effect of liposome charge and PEG polymer layer thickness on cell-liposome electrostatic interactions. Biochim Biophys Acta. 2002; 1564:343. [PubMed: 12175916]
56. Kurnik BR, Huskey M, Hagerty D, Hruska KA. Vitamin D metabolites stimulate phosphatidylcholine transfer to renal brush-border membranes. Biochim Biophys Acta. 1986; 858:47. [PubMed: 3754768]
57. Hoekstra LT, de Graaf W, Nibourg GAA, Heger M, Bennink RJ, Stieger B, van Gulik TM. Physiological and biochemical basis of clinical liver function tests. Ann Surg. 2012; 257:1.
58. Leffell DJ, Thompson JT. Lasers in dermatology and ophthalmology. Dermatol Clin. 1992; 10:687. [PubMed: 1395152]
59. Verkruysse W, Lucassen GW, van Gemert MJ. Simulation of color of port wine stain skin and its dependence on skin variables. Lasers Surg Med. 1999; 25:131. [PubMed: 10455219]
60. Lucassen GW, Verkruysse W, Keijzer M, van Gemert MJ. Light distributions in a port wine stain model containing multiple cylindrical and curved blood vessels. Lasers Surg Med. 1996; 18:345. [PubMed: 8732573]
61. Verkruysse W, Pickering JW, Beek JF, Keijzer M, van Gemert MJ. Modeling the effect of wavelength on the pulsed dye laser treatment of port wine stains. Appl Opt. 1993; 32:393. [PubMed: 20802703]
62. van Gemert MJ, Smithies DJ, Verkruysse W, Milner TE, Nelson JS. Wavelengths for port wine stain laser treatment: Influence of vessel radius and skin anatomy. Phys Med Biol. 1997; 42:41. [PubMed: 9015807]
63. Greve B, Raulin C. Prospective study of port wine stain treatment with dye laser: Comparison of two wavelengths (585 nm vs. 595 nm) and two pulse durations (0.5 milliseconds vs. 20 milliseconds). Lasers Surg Med. 2004; 34:168. [PubMed: 15004830]
64. Kelly KM, Nanda VS, Nelson JS. Treatment of port-wine stain birthmarks using the 1.5-msec pulsed dye laser at high fluences in conjunction with cryogen spray cooling. Dermatol Surg. 2002; 28:309. [PubMed: 11966787]
65. Gaber MH, Hong K, Huang SK, Papahadjopoulos D. Thermosensitive sterically stabilized liposomes: Formulation and *in vitro* studies on mechanism of doxorubicin release by bovine serum and human plasma. Pharm Res. 1995; 12:1407. [PubMed: 8584472]
66. Yang T, Cui FD, Choi MK, Cho JW, Chung SJ, Shim CK, Kim DD. Enhanced solubility and stability of PEGylated liposomal paclitaxel: *In vitro* and *in vivo* evaluation. Int J Pharm. 2007; 338:317. [PubMed: 17368984]

Author Manuscript Author Manuscript Author Manuscript Author Manuscript

67. Sun W, Zou W, Huang G, Li A, Zhang N. Pharmacokinetics and targeting property of TFu-loaded liposomes with different sizes after intravenous and oral administration. J Drug Target. 2008; 16:357. [PubMed: 18569280]

68. Marsh D. General features of phospholipid phase transitions. Chem Phys Lipids. 1991; 57:109.

69. Evans EA, Waugh R. Mechano-chemistry of closed, vesicular membrane systems. J Colloid Interface Sci. 1977; 60:286.

70. Nagle JF, Scott HL. Lateral compressibility of lipid mono-and bilayers. Theory of membrane permeability. Biochim Biophys Acta. 1978; 513:236. [PubMed: 718892]

71. Doniach S. Thermodynamic fluctuations in phospholipid bilayers. J Chem Phys. 1978; 68:4912.

72. Miles LA, Plow EF. Binding and activation of plasminogen on the platelet surface. J Biol Chem. 1985; 260:4303. [PubMed: 3920216]

73. Levin EG, Santell L, Osborn KG. The expression of endothelial tissue plasminogen activator *in vivo*: A function defined by vessel size and anatomic location. J Cell Sci. 1997; 110:139. [PubMed: 9044044]

74. Markus G, Priore RL, Wissler FC. The binding of tranexamic acid to native (Glu) and modified (Lys) human plasminogen and its effect on conformation. J Biol Chem. 1979; 254:1211. [PubMed: 762124]

75. Nguyen CM, Yohn JJ, Huff C, Weston WL, Morelli JG. Facial port wine stains in childhood: Prediction of the rate of improvement as a function of the age of the patient, size and location of the port wine stain and the number of treatments with the pulsed dye (585 nm) laser. Br J Dermatol. 1998; 138:821. [PubMed: 9666828]

Author Manuscript Author Manuscript Author Manuscript Author Manuscript

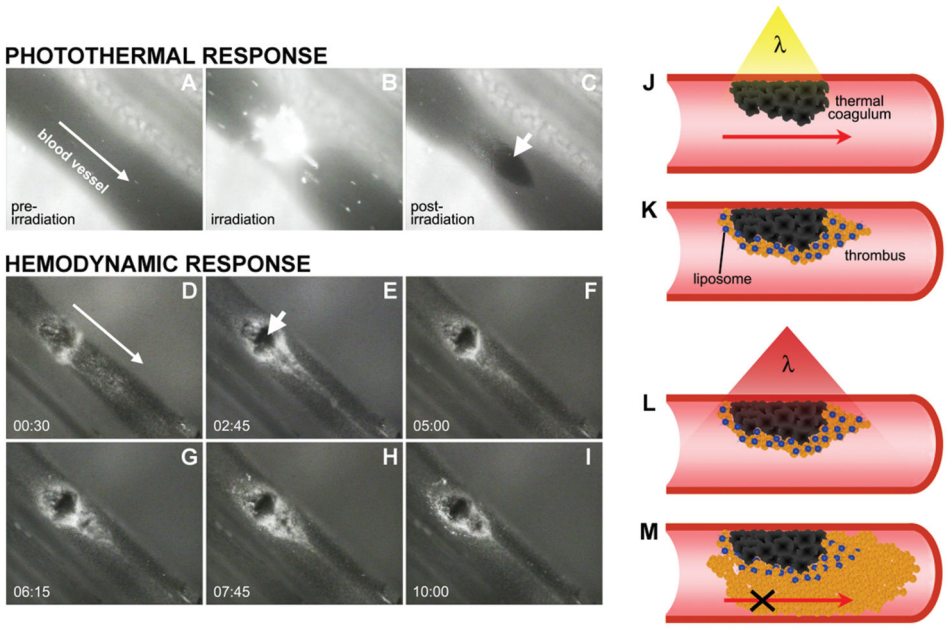

Figure 1.

Endovascular laser-tissue interactions and the principles of site-specific pharmaco-laser therapy (SSPLT).

Notes: Endovascular laser-tissue interactions are demonstrated in laser-irradiated hamster dorsal skin fold venules (A–I). The first component of endovascular laser-tissue interactions is the photothermal response (A–C), where laser irradiation of a blood vessel (A, arrow indicates direction of blood flow, and B) with a wavelength predominantly absorbed by hemoglobin results in the formation of a thermal coagulum (C, arrow). The photothermal response subsequently triggers the hemodynamic response (D–I), characterized by platelet aggregation and initiation of the coagulation cascade that culminates in the formation of a thrombus (fluorescently labeled) around the thermal coagulum (E, arrow). Thermal coagula were induced as previously described and thrombi were stained with 5(6)-carboxyfluorescein for visualization by intravital fluorescence microscopy.[14, 15, 32, 52] The elapsed time (min:sec) after the laser pulse is indicated in the lower left corner. The principles of SSPLT (J–M) are predicated on both components of endovascular laser-tissue interactions. The photothermal response (J), induced by yellow laser irradiation (J, λ), is followed by a hemodynamic response (orange spheres = platelets) that is amplified by the infusion of a thrombus-targeting prothrombotic and/or antifibrinolytic agent-containing drug carrier, such as thermosensitive liposomes (K, blue spheres). Thrombus targeting can be achieved by liposome-conjugated antibodies directed against epitopes on activated platelets (e.g., CD41, CD62P) or fibrin (K).[12] Following liposome accumulation, drug release can be induced by local heating, e.g., by a second near-infrared laser pulse (L, λ).[29] The arrows in (J) and (M) indicate blood flow; the '*X*' in (M) designates cessation of blood flow. Data presented in panels A–I were taken from previous studies by our group.[14, 15]

Author Manuscript Author Manuscript Author Manuscript Author Manuscript

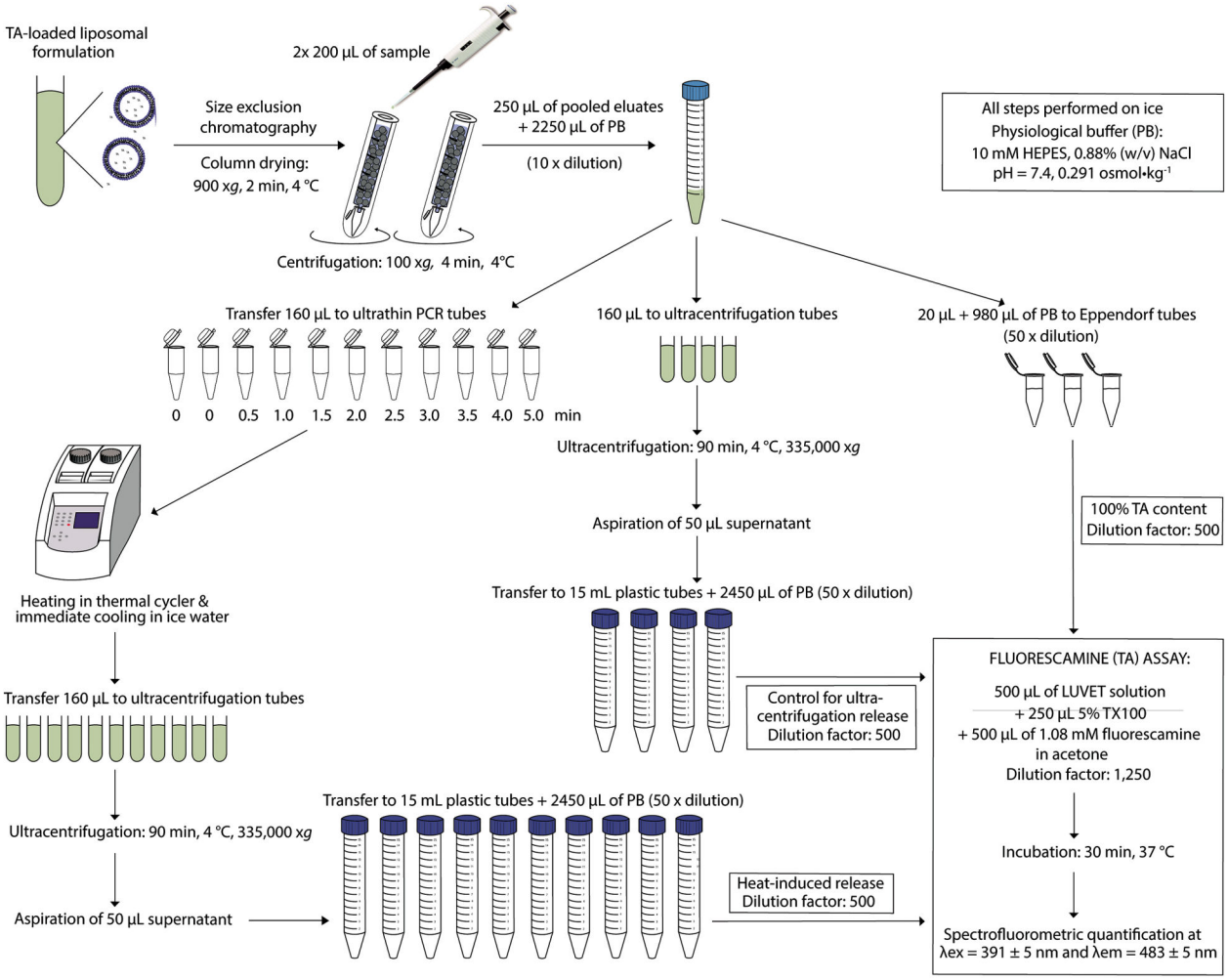

Figure 2.

Schematic overview of the protocol used to determine heat-induced tranexamic acid release in buffer.

Author Manuscript Author Manuscript Author Manuscript Author Manuscript

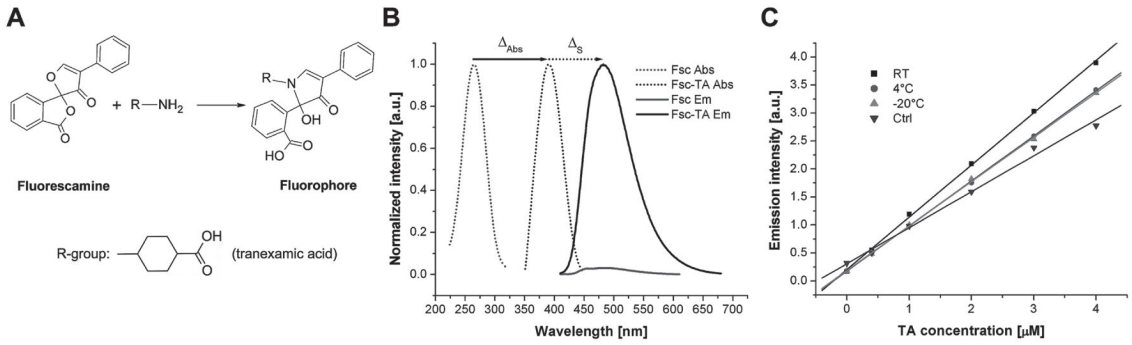

Figure 3.

(A) Fluorescamine reacts with compounds containing a primary amino group, such as TA, to form fluorescent pyrrolinone-type moieties. Unreacted fluorescamine is hydrolyzed to form non-fluorescent reaction products. (B) Normalized (to maximum) absorbance and emission spectra of unreacted fluorescamine (Fsc Abs and Fsc Em, respectively) and fluorescamine reacted with TA (Fsc-TA Abs and Fsc-TA Em, respectively). The relative intensities between Fsc Em and Fcs-TA Em were maintained to show the lack of fluorescence of the former. (C) TA was derivatized with fluorescamine in the presence of 1% Triton-X 100 and incubated for 30 min at RT (Ctrl) or for 24 h at RT, 4 °C, or −20 °C. The emission intensity [arbitrary units] is plotted versus TA concentration within the TA calibration range as used in all experiments.

Notes: Abbreviations: RT, room temperature; Ctrl, control; TA, tranexamic acid; Fsc, fluorescamine; Abs, absorption spectrum; Em, emission spectrum.

Author Manuscript Author Manuscript Author Manuscript Author Manuscript

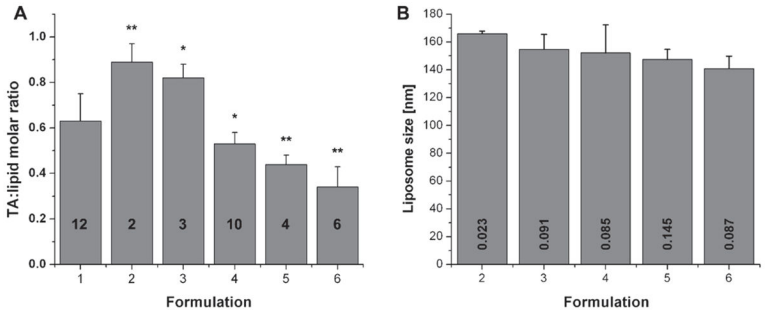

Figure 4.

TA:lipid ratios (A) and LUVET sizes (B) plotted for the six formulations assayed: 1: DPPC; 2: DPPC:DSPE-PEG (98:2 molar ratio); 3: DPPC:DSPE-PEG (96:4); 4: DPPC:DSPE-PEG (94:6); 5: DPPC:MPPC (90:10); and 6: DPPC:MPPC:DSPE-PEG2000 (86:10:4).

Notes: Drug:lipid ratios were calculated by dividing the TA concentration as determined by the fluorescamine assay by the phospholipid concentration as determined by the Rouser assay as detailed in the experimental section. In (A) and (B), the numbers inside the bars indicate sample size and polydispersity index, respectively. Values are plotted as mean±SD. In (A), the level of significance is indicated versus control.

Author Manuscript Author Manuscript Author Manuscript Author Manuscript

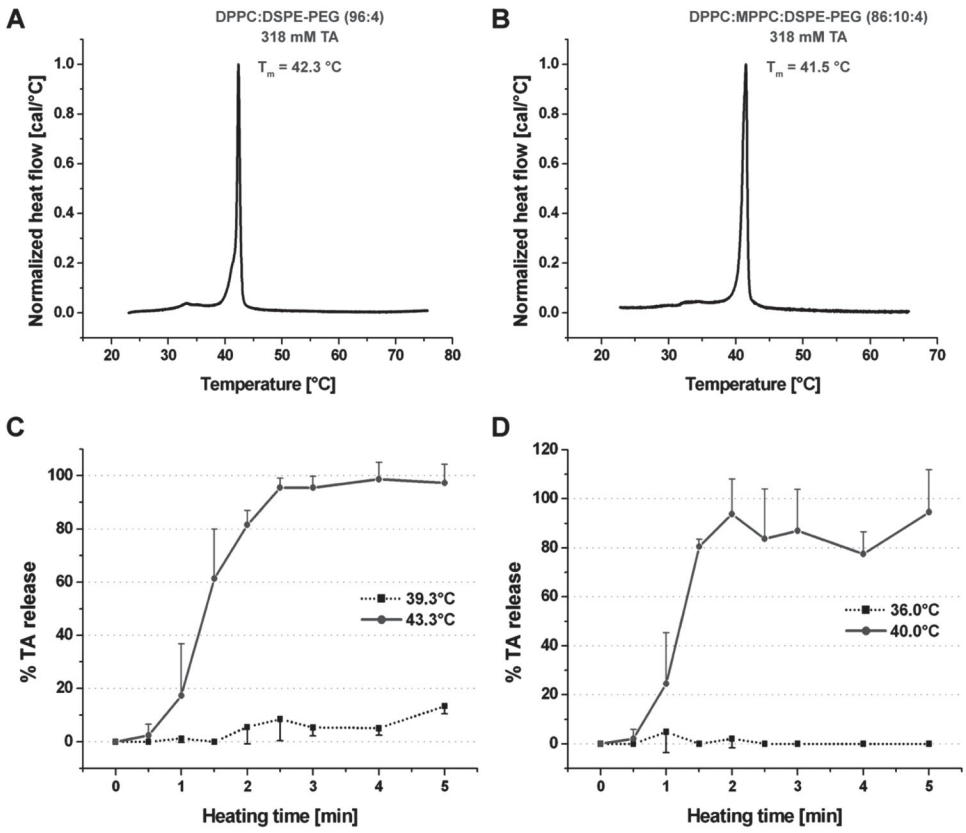

Figure 5.

DSC thermograms of TA-encapsulating DPPC:DSPE-PEG (96:4) (A) and DPPC:MPPC:DSPE-PEG (86:10:4) (B) LUVETs. (C) Heat-induced TA release from DPPC:DSPE-PEG (96:4) LUVETs plotted versus heating time at 39.3 °C (dotted line) and 43.3 °C (solid line). (D) Heat-induced TA release from DPPC:MPPC:DSPE-PEG (86:10:4) LUVETs plotted versus heating time at 36.0 °C (dotted line) and 40.0 °C (solid line). Released TA concentration is expressed as a mean±SD percentage of total liposomal TA concentration ($N = 3$ per time point). *Abbreviation:* T_m, phase transition temperature.

Author Manuscript Author Manuscript Author Manuscript Author Manuscript

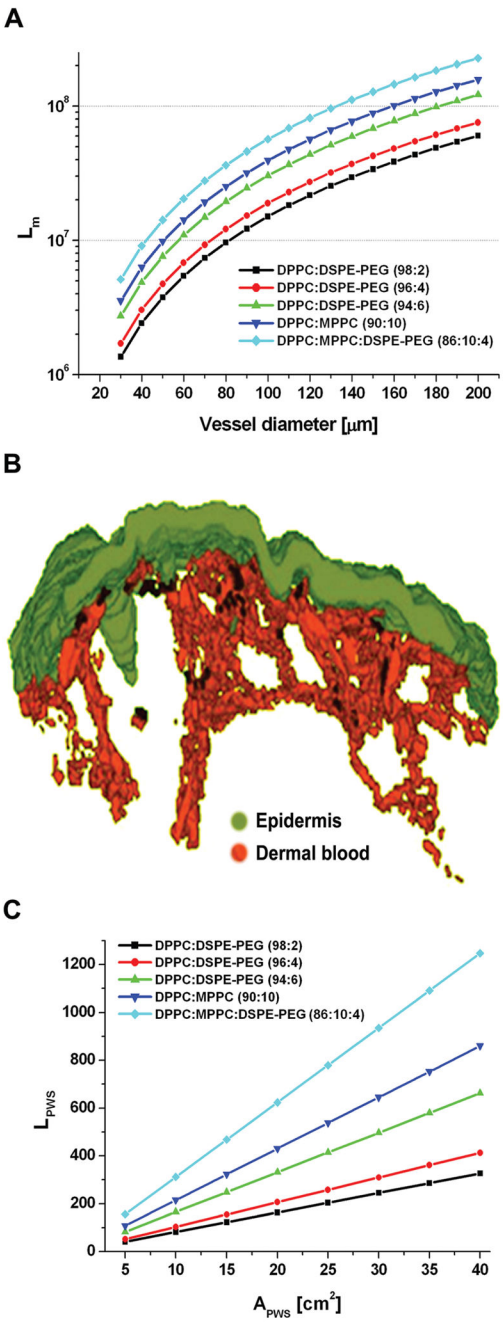

Figure 6.

(A) The number of LUVETs minimally required to achieve a TA concentration of 1.9 mM in a 500-μm long vessel segment, plotted as a function of vessel diameter. (B) 3D histological reconstruction of a PWS biopsy from Smithies et al.,[39] from which (C) the number of minimally required LUVETs for a port wine stain was derived as a function of port wine stain surface area. *Abbreviations:* L_m, number of minimally required LUVETs; L_{pws}, number of minimally required LUVETs for a port wine stain; A_{PWS}, port wine stain surface area.

Author Manuscript Author Manuscript Author Manuscript Author Manuscript

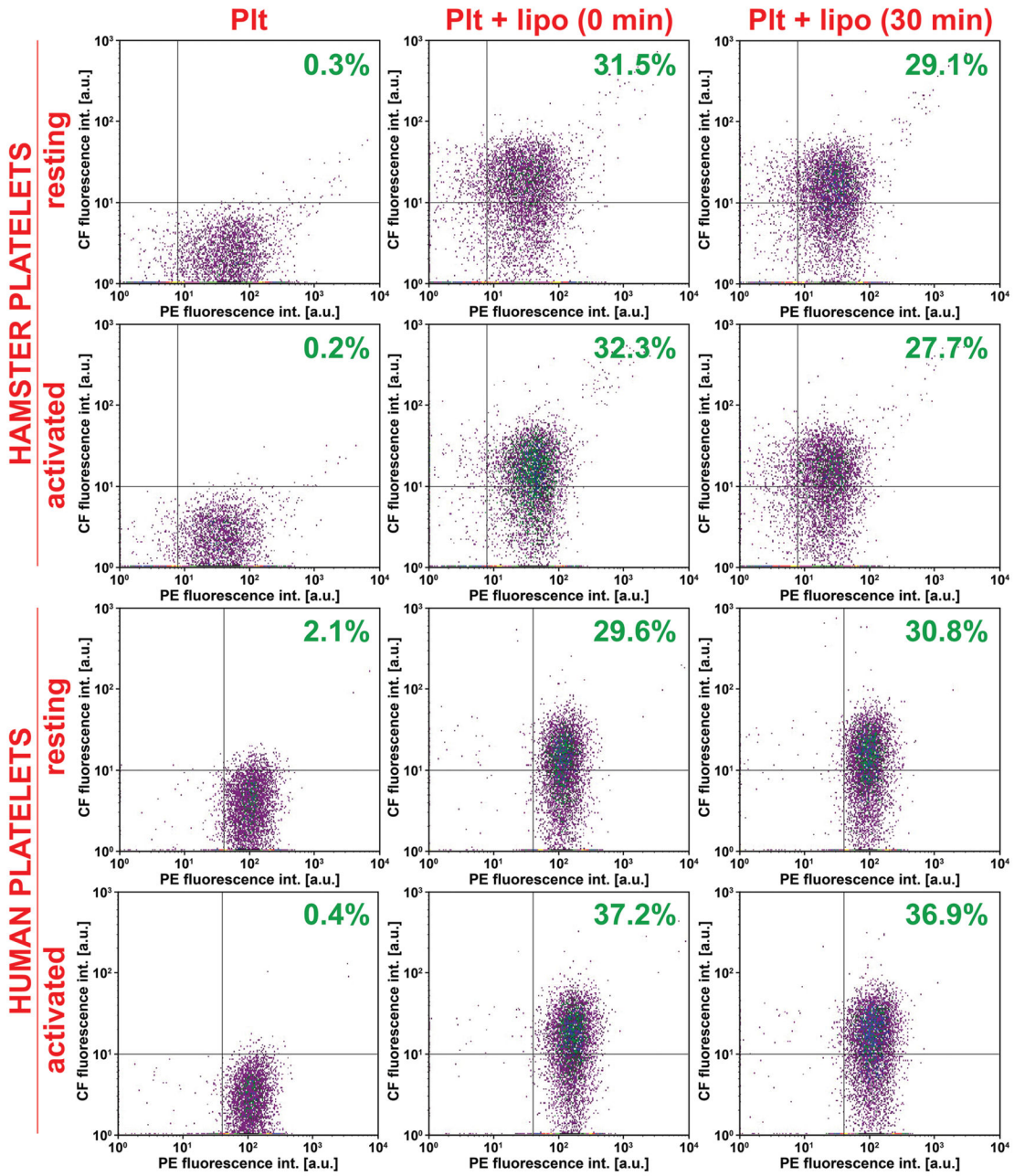

Figure 7.

Representative density plots of isolated resting and activated hamster and human platelets (Plt) assayed either without incubation with *F3* CF-encapsulating LUVETS (left column) or after addition of LUVETs that were directly washed away (central column) or incubated with the platelets for 30 min (right column). The platelets were counterstained with PE-conjugated anti CD42b (hamster) or CD61 (human) antibodies (*x*-axis). The fraction of PE- and CF-positive platelets in the upper right quadrant is indicated in green in the respective quadrant. The population of cells represents the gated cell population from the forward (FS)- and sideways scatter 2D plots. *Abbreviation*: Plt, platelets.

Author Manuscript Author Manuscript Author Manuscript Author Manuscript

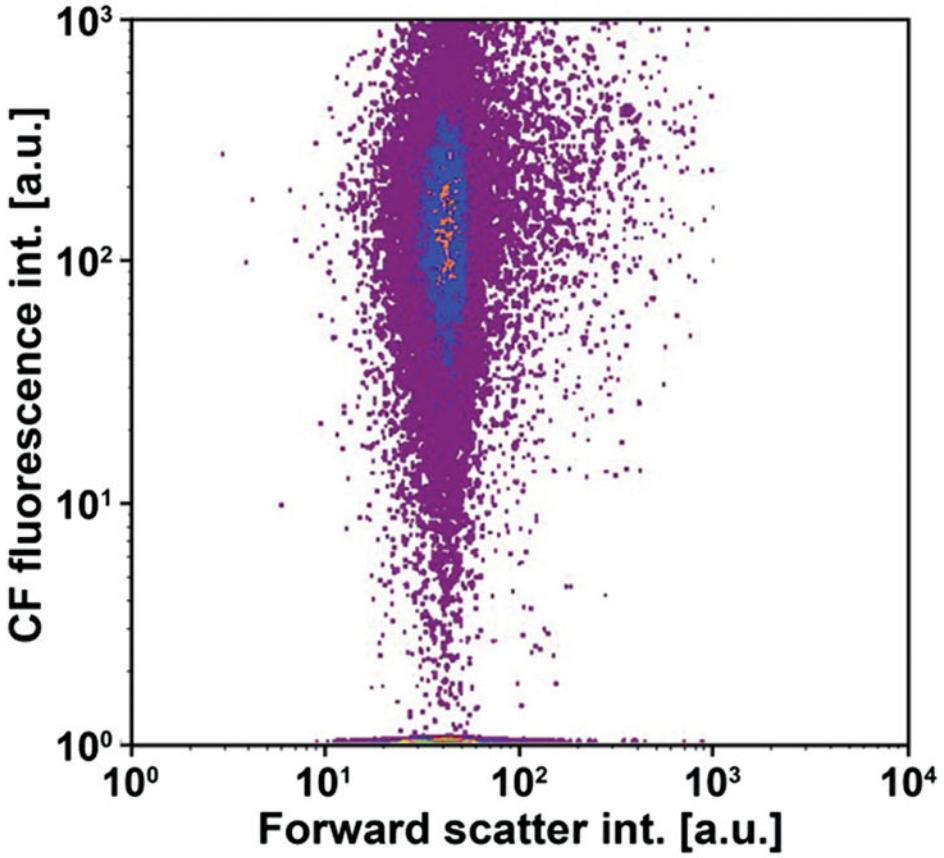

Figure 8.

Representative flow cytometry density plot of CF-encapsulating *F3* LUVETs that were used in the *in vitro* LUVET-platelet and LUVET-red blood cell association/uptake studies, showing the intense fluorescence signal in the FL1 channel (CF fluorescence, *y*-axis). *Abbreviation*: CF, 5(6)-carboxyfluorescein.

Author Manuscript Author Manuscript Author Manuscript Author Manuscript

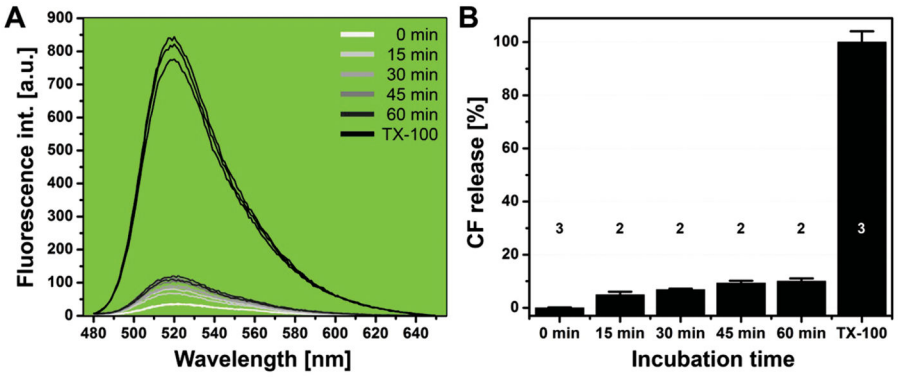

Figure 9.

Passive release of CF from *F3* LUVETs incubated for increasing periods of time at 37 °C or after addition of TX-100. (A) Fluorescence emission spectra of CF in the supernatant of ultracentrifuged samples. (B) Calculated percentage of passive CF release as a function of incubation time. The percentage of release was calculated on the basis of the CF peak integrals (480–650 nm) and expressed as (fluorescence intensity of sample–fluorescence intensity of negative control)/(fluorescence intensity of positive control–fluorescence intensity of negative control) × 100%. The numbers above/in the bar(s) indicate the sample size. *Abbreviation*: CF, 5(6)-carboxyfluorescein.

Author Manuscript Author Manuscript Author Manuscript Author Manuscript

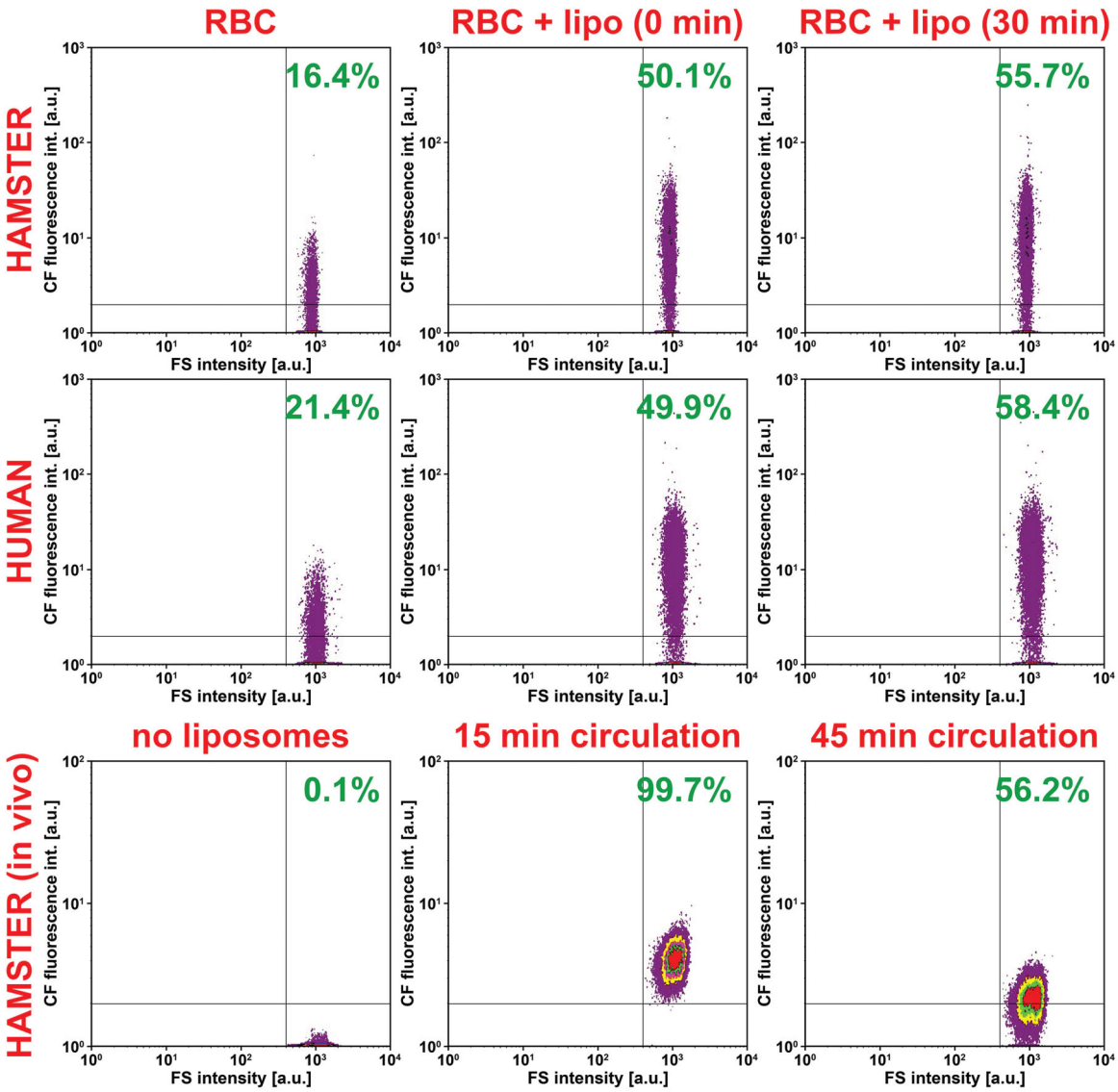

Figure 10.

(Upper and middle row) Representative density plots of gated hamster and human RBCs assayed either without incubation with *F3* CF-encapsulating LUVETS (left column) or after addition of LUVETs that were directly washed away (central column) or incubated with the platelets for 30 min (right column). (Bottom row) Density plots of washed RBCs isolated from hamsters without infusion of *F3* NBD-labeled LUVETs (left panel) or 15 min (central panel) or 45 min (right panel) after infusion of NBD-LUVETs. In all panels, the percentage of CF- and NBD-positive RBCs in the upper right quadrant is indicated in green. Also, the population of cells represents the gated cell population from the forward (FS)- and sideways scatter 2D plots. *Abbreviation*: RBC, red blood cells.

Author Manuscript Author Manuscript Author Manuscript Author Manuscript

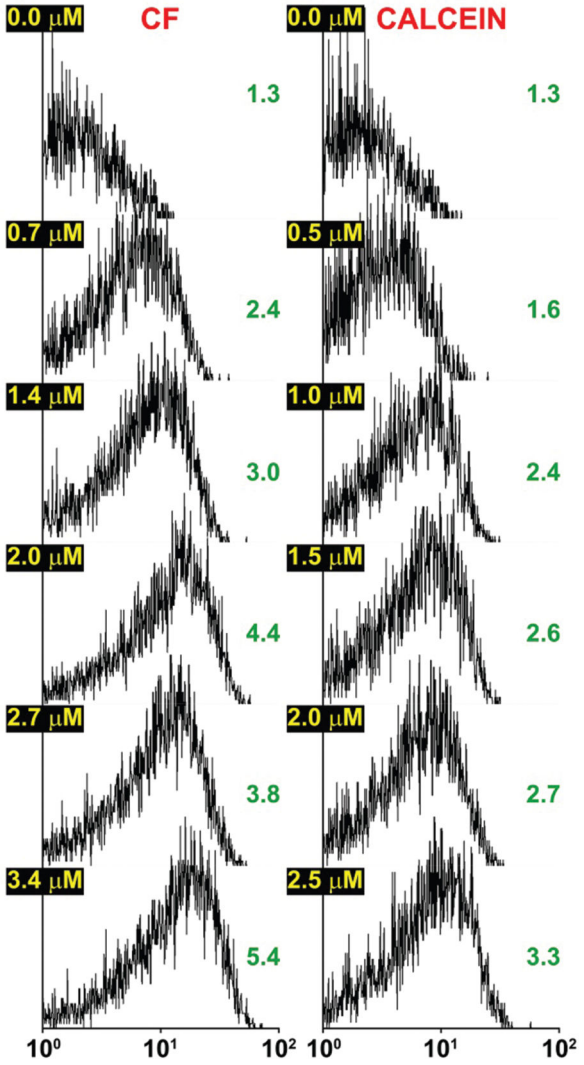

Figure 11.

Uptake/association of unencapsulated CF and calcein by/with human red blood cells, presented as flow cytometry histograms as a function of fluorophore concentration (yellow values in black boxes). The mean FL1 fluorescence, plotted on the *x*-axis and indicative of CF and calcein fluorescence, is provided in green values on the right of the histogram. Data were obtained with a single population of red blood cells. *Abbreviation*: CF, 5(6)-carboxyfluorescein.

Author Manuscript Author Manuscript Author Manuscript Author Manuscript

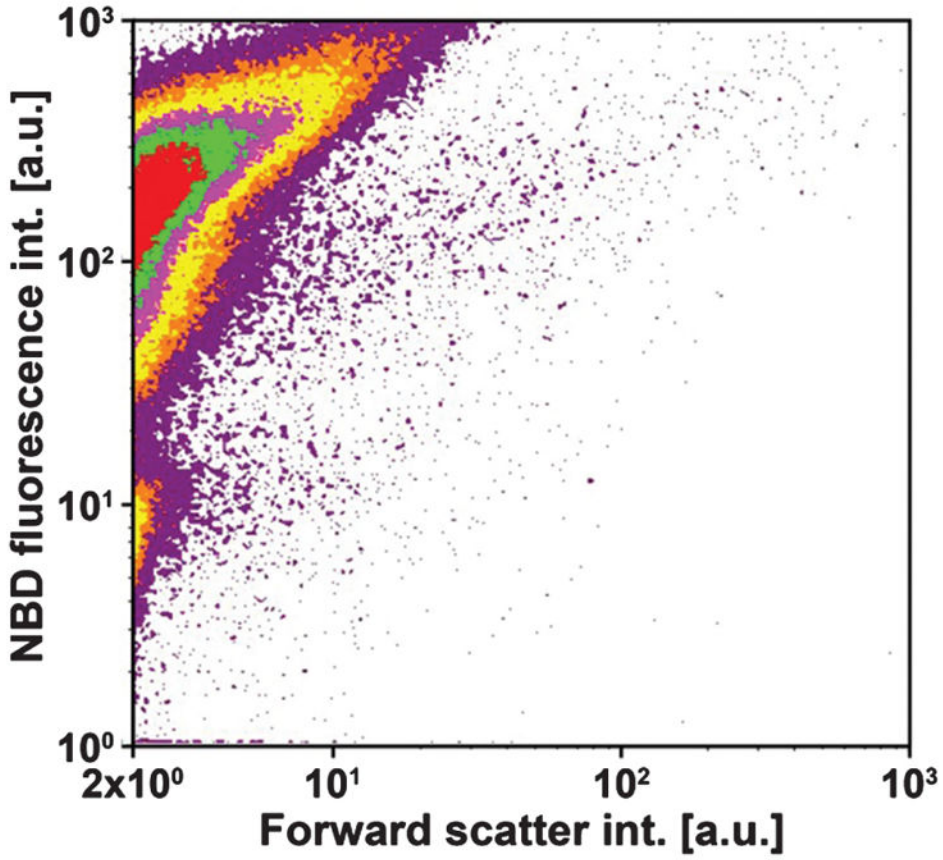

Figure 12.

Representative flow cytometry density plot of NBD-labeled *F3* LUVETs that were used in the *in vivo* LUVET-red blood cell association/uptake studies, showing the intense fluorescence signal in the FL1 channel (NBD fluorescence, *y*-axis).

Author Manuscript Author Manuscript Author Manuscript Author Manuscript

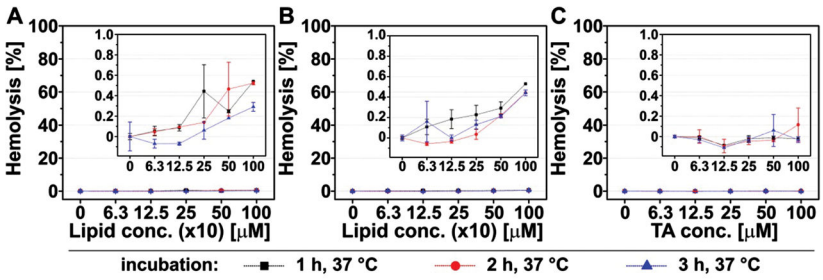

Figure 13.

Lytic effects of *F3* LUVETs (A), TA-encapsulating *F3* LUVETs (B), and TA (C) on human red blood cells. The extent of hemolysis was expressed as $((OD_{sample} - \text{mean } OD_{negative\ control})/(\text{mean } OD_{positive\ control} - \text{mean } OD_{negative\ control}) \times 100\%$, whereby the level of free hemoglobin in centrifuged cell supernatants was determined spectrophotometrically at 577 nm. Cells were incubated with LUVETs or TA as indicated in the legend below the panels. Each data point represents the mean±variance of $N=2$ samples. *Abbreviation*: OD, optical density.

Author Manuscript Author Manuscript Author Manuscript Author Manuscript

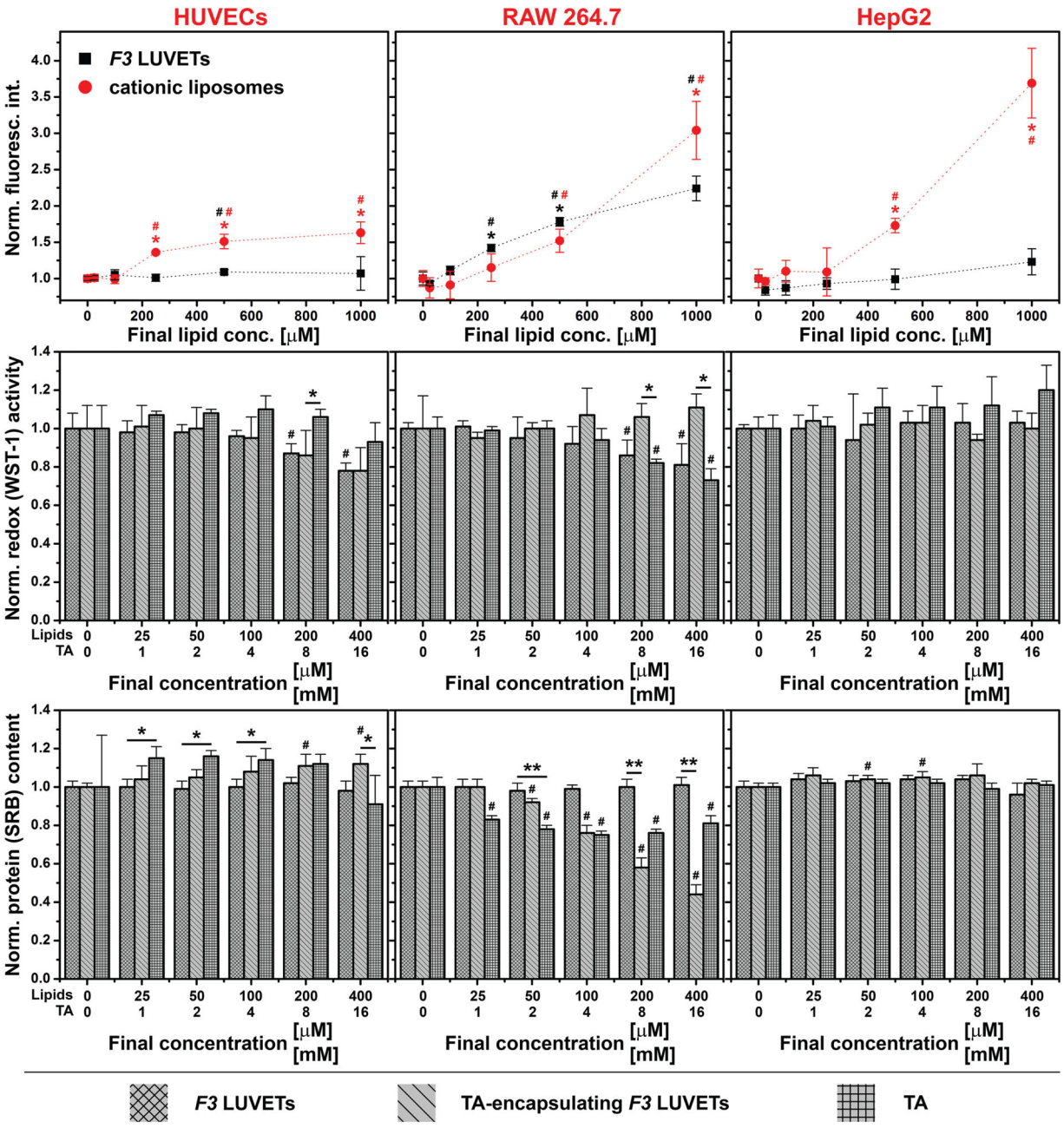

Figure 14.

Summary of lipid concentration-dependent uptake (upper row) and lipid- and TA concentration-dependent toxicity (center and bottom row) of *F3* LUVETs in cultured HUVECs (left column), RAW 264.7 macrophages (center column), and HepG2 hepatocytes (right column). For the uptake assays, the fluorescence intensity of cells was used as a measure of uptake of fluorescently labeled *F3* LUVETs (not containing TA) and fluorescently labeled cationic liposomes (positive control) ($N = 4$ per concentration). Data were normalized to the cells' autofluorescence (0 μM lipids/LUVETs). For the toxicity assays, WST-1 conversion and protein content (SRB assay) were determined as a measure of

Author Manuscript Author Manuscript Author Manuscript Author Manuscript

mitochondrial redox potential and cell viability ($N = 4$ per lipid or TA concentration). The lipid concentration on the *x*-axis pertains to LUVETs and gelfiltered TA-encapsulating LUVETs. Data were normalized to the 0-μM controls. The legend for the cytotoxicity panels is provided at the bottom. Values are plotted as mean±SD. $^{\#}$Designates $p \leq 0.05$ versus control (0), whereas * and ** indicate intergroup differences with $p \leq 0.05$ and $p \leq 0.01$, respectively. For the uptake data, the significance symbols are color-coded (black = *F3* LUVETs, red = cationic liposomes).

Author Manuscript

Author Manuscript

Author Manuscript

Author Manuscript

Table I

The number of minimally required LUVETs indicated per μL blood for every SSPLT candidate formulation.

Formulation (mol%)	$L_m \cdot \mu L^{-1}$
2 DPPC:DSPE-PEG2000 (98:2)	3.8
3 DPPC:DSPE-PEG2000 (96:4)	4.8
4 DPPC:DSPE-PEG2000 (94:6)	7.7
5 DPPC:MPPC (90:10)	10.0
6 DPPC:MPPC:DSPE-PEG2000 (86:10:4)	14.5

Notes: Values are predicated on 100% TA release from thermosensitive LUVETs. *Abbreviation:* L_m, number of minimally required LUVETs.

Author Manuscript

Author Manuscript

Author Manuscript

Author Manuscript

Table II

The encapsulation efficiency, trapped volume, and endovesicular TA concentration of the assayed formulations.

Formulation (mol%)	E_{eff} (%)	V_t [L · mol^{-1}]	C_{TA} [M]
1 DPPC	0.98	26.09	0.024
2 DPPC:DSPE-PEG2000 (98:2)	1.40	4.11	0.217
3 DPPC:DSPE-PEG2000 (96:4)	1.29	3.84	0.214
4 DPPC:DSPE-PEG2000 (94:6)	0.83	3.78	0.140
5 DPPC:MPPC (90:10)	0.70	3.72	0.119
6 DPPC:MPPC:DSPE-PEG2000 (86:10:4)	0.53	3.56	0.095

Notes: Abbreviations: E_{eff}, encapsulation efficiency; V_t , trapped volume; C_{TA}, endovesicular TA concentration.

Author Manuscript Author Manuscript Author Manuscript Author Manuscript

Table III

List of parameters derived from experimental data that were used to calculate the C_{TA}.

Formulation (mol%)	OM surface (nm^2)	IM surface (nm^2)	No. of lipids OM	No. of lipids IM	Lipids per vesicle	TA molecules per vesicle	eV_t (L/vesicle)
1 DPPC	3,480,638	3,428,839	7,045,825	6,940,969	13,986,794	8,744,807	6.06×10^{-16}
2 DPPC:DSPE-PEG2000 (98:2)	86,500	78,498	175,059	158,864	333,923	298,165	2.28×10^{-18}
3 DPPC:DSPE-PEG2000 (96:4)	75,167	67,720	152,085	137,019	289,104	237,516	1.84×10^{-18}
4 DPPC:DSPE-PEG2000 (94:6)	72,804	65,478	147,269	132,451	279,720	147,848	1.75×10^{-18}
5 DPPC:MPPC (90:10)	68,315	61,225	135,923	121,817	257,740	114,195	1.59×10^{-18}
6 DPPC:MPPC:DSPE-PEG2000 (86:10:4)	62,474	55,703	124,213	110,750	234,963	79,027	1.39×10^{-18}

Notes: In order to calculate the C_{TA}, the number of TA molecules per LUVET and the eV_t had to be derived from the mean LUVET sizes, the phospholipid molecular areas, and the measured TA:lipid ratios. The calculation method for each parameter is described in the experimental section. *Abbreviations*: OM, outer membrane; IM, inner membrane; No., number; Q_{TA}, quantity of TA molecules per vesicle; eV_t , trapped volume per vesicle.

J Biomed Nanotechnol. Author manuscript; available in PMC 2017 August 01.

Author Manuscript

Author Manuscript

Author Manuscript

Author Manuscript

Table IV

Summary of *F3* LUVET-platelet association.

	Flu. intensity [a.u.]	URQ cells [%]	*N*
Hamster platelets			
RESTING			
Platelets	1.3 ± 0.1	0.6 ± 0.7	3
Platelets+ LUVETs, 0 min	3.9 ± 0.2	31.4 ± 1.0	3
Platelets+ LUVETs, 30 min	3.6 ± 0.4	29.3 ± 4.4	3
ACTIVATED			
Platelets	1.6 ± 0.6	1.3 ± 1.1	3
Platelets+ LUVETs, 0 min	4.4 ± 0.4	34.3 ± 3.0	3
Platelets+ LUVETs, 30 min	4.6 ± 0.8	35.2 ± 6.5	3
Human platelets			
RESTING			
Platelets	1.5 ± 0.2	1.2 ± 1.1	4
Platelets+ LUVETs, 0 min	3.9 ± 0.3	33.3 ± 3.1	3
Platelets+ LUVETs, 30 min	3.7 ± 0.1	31.6 ± 0.9	4
ACTIVATED			
Platelets	1.5 ± 0.1	1.2 ± 0.7	4
Platelets+ LUVETs, 0 min	4.9 ± 0.6	37.3 ± 0.6	3
Platelets+ LUVETs, 30 min	5.8 ± 1.0	41.7 ± 3.0	4

Notes: The analysis was performed on gated cells. The parameters of the quadrants were: *x*-axis (PE fluorescence): 8, *y* -axis (CF fluorescence): 10 for hamster platelets and *x*-axis: 40, *y* -axis: 10 for human platelets, which are shown in Figure 7. *Abbreviations*: Flu., fluorescence; a.u., arbitrary units; URQ, upper right quadrant.

Author Manuscript

Author Manuscript

Author Manuscript

Author Manuscript

Table V

Summary of *in vitro F3* LUVET-red blood cell association.

	Flu. intensity [a.u.]	URQ cells [%]	*N*
Hamster red blood cells			
RBCs	1.3 ± 0.0	15.5 ± 1.2	2
RBCs+ LUVETs, 0 min	4.4 ± 2.0	57.3 ± 10.2	2
RBCs+ LUVETs, 30 min	4.6 ± 1.5	57.9 ± 3.2	2
Human red blood cells			
RBCs	1.3 ± 0.1	19.2 ± 3.2	2
RBCs+ LUVETs, 0 min	3.2 ± 0.5	51.5 ± 2.3	2
RBCs+ LUVETs, 30 min	4.0 ± 0.3	56.5 ± 2.6	2

Notes: The analysis was performed on gated cells. The parameters of the quadrants were: *x*-axis (forward scatter intensity): 400, *y* -axis (CF fluorescence): 2 for both hamster and human red blood cells, which are shown in Figure 10. *Abbreviations*: Flu., fluorescence; a.u., arbitrary units; URQ, upper right quadrant.